Modeling and Assessment of Efficiency in Arbitrary Air-Breathing Power Systems

by

Wyatt Giroux

Submitted to the Department of Aeronautics and Astronautics
in partial fulfillment of the requirements for the degree of

MASTER OF SCIENCE IN AERONAUTICS AND ASTRONAUTICS

at the

MASSACHUSETTS INSTITUTE OF TECHNOLOGY

May 2024

Authored by: Wyatt Giroux
Department of Aeronautics and Astronautics
May 16, 2024

Certified by: Raymond L. Speth
Principal Research Scientist, Thesis Supervisor

Accepted by: Jonathan P. How
R.C. Maclaurin Professor of Aeronautics and Astronautics
Chair, Graduate Program Committee

Modeling and Assessment of Efficiency in Arbitrary Air-Breathing Power Systems

by

Wyatt Giroux

Submitted to the Department of Aeronautics and Astronautics
on May 16, 2024 in partial fulfillment of the requirements for the degree of

MASTER OF SCIENCE IN AERONAUTICS AND ASTRONAUTICS

ABSTRACT

The push for net-zero carbon emissions in the aviation sector by 2050 has resulted in an increasing amount of work being done to analyze the benefits of emergent technologies. Aircraft propulsion systems are a common subject of such research, and studies of some proposed architectures, such as hybrid-electric powertrains, have suggested potential fuel-burn and nitrogen oxide emissions reductions of up to 10% and 4.9%, respectively. When attempting to refine and compare these systems, efficiency is a commonly used metric. Efficiency models provide an understanding of where and how energy is being dissipated in a given system, making them invaluable design and evaluation tools. Until recently, the traditional thermal/propulsive efficiency breakdown has been used to model gas-turbine engines. However, this model has two major deficiencies. First, the lack of a per-component efficiency model restricts understanding of system energy dissipation to either thermodynamic or propulsive losses. Second, the traditional model is unable to capture systems utilizing additional energy sources (batteries, fuel cells, etc.) and their respective conversion pathways. While individual studies have created efficiency models for unconventional systems, these models are either specific to a given architecture or are only applicable to a specific class of engines. This makes comparison between specific terms in existing efficiency models impossible.

This thesis presents the Modular Efficiency Model (MEM), which is capable of constructing low-level efficiency models that accurately represent energy flow pathways and are algebraically consistent across arbitrary collections of propulsion system components. This is done by tracking the kinetic energy flow available for propulsion (expanded flow power) across each component in a system. MEM provides a more detailed breakdown of useful energy dissipation, relative influence of streams and components, and individual powertrain efficinecies that can be meaningfully compared to other systems. MEM is demonstrated in this work by comparing performance of unmixed, mixed-flow, and hybrid electric engine architectures. We identify high fan pressure ratio systems with low fan diameter as candidates for effective mixer use. For hybrid-electric systems, we find a 3.2% reduction in whole-mission fuel burn is possible at the cost of carrying only 50% of the original aircraft payload. Numerous detailed future studies utilizing MEM are recommended, using this thesis as a baseline example for the use of MEM in analyzing and comparing novel architectures.

Thesis supervisor: Raymond L. Speth
Title: Principal Research Scientist

Acknowledgments

I would like to thank my research advisor, Dr. Raymond Speth, and the entire ASCENT 47 team for guiding this first-generation graduate through the vast ocean that is research. A special thanks to Dr. Prakash Prashanth in particular for putting up with my random drop-ins followed by hours of fruitless troubleshooting only for me to figure out the offending issues as soon as we stopped. Without the team's help and expertise, I would have gotten hopelessly lost quite a while ago. I would like to thank Steven Barrett for his help as my academic advisor as well as the FAA for funding this project. I'd also like to thank my friends in the Lab for Aviation and the Environment for all the fun we had in between bursts of stress.

Finally, I'd like to thank my friends and family who have supported me throughout my undergraduate years and now through the first leg of the marathon that is graduate school. Here's to the end of this journey and the beginning of the PhD adventure!

Contents

List of Figures

List of Tables

Nomenclature

Symbols

B_p	Leakage bleed extraction fraction [$\sim$]
c_p	Specific heat at constant pressure [J kg^{-1} K^{-1}]
E	Source energy [J]
E^*	Battery specific energy [Wh kg^{-1}]
E_p	Flow power extraction fraction [$\sim$]
F_N	Net thrust [N]
h	Static specific enthalpy [J kg^{-1}]
h_t	Total specific enthalpy [J kg^{-1}]
H_F	Degree of thrust hybridization [$\sim$]
H_p	Degree of power hybridization [$\sim$]
LHV	Fuel lower heating value [J kg^{-1}]
$\dot{m}$	Mass flow rate [kg s^{-1}]
P	Source power [W]
P^*	Battery specific power [W kg^{-1}]
R	Ideal gas constant for air [J kg^{-1} K^{-1}]
u	Flow speed [m s^{-1}]
$\dot{W}$	Shaft power [W]
x	Specific exergy [J kg^{-1}]
α	Bypass ratio [$\sim$]
γ	Specific heat ratio [$\sim$]
$\delta\eta$	Relative power dissipation [$\sim$]
ϵ^{st}	Stream power fraction [$\sim$]

ϵ^{sh}	Shaft power fraction [$\sim$]
ε^{st}	Stream power fraction ratio [$\sim$]
$\hat{\varepsilon}^{st}$	Specific stream power fraction ratio [$\sim$]
ζ	Exergy efficiency [$\sim$]
η	Component flow power efficiency [$\sim$]
η_0	Overall efficiency [$\sim$]
η_p	Propulsive efficiency [$\sim$]
η_{is}	Component isentropic efficiency [$\sim$]
κ	Static loss fraction [$\sim$]
σ	Expanded flow power [W]
$\hat{\sigma}$	Specific expanded flow power [W kg^{-1}]
$\Delta\sigma$	Expanded flow power rise [W]
χ	Component effectiveness [$\sim$]

Subscripts

amb	Ambient
bat	Battery
$diff$	Mechanical differential
ext	Flow power extractor
fan	Fan
f	Fuel
fpp	Flow power producer
gg	Gas generator
gen	Electric generator
i	Indexing variable
$i-j$	Quantity at station i minus quantity at station j
$(\cdot)_{k-\ell}^{i-j}$	Ratio of two differences
in	Inlet
inp	Total input to a component
j	Indexing variable

k	Indexing variable
ℓ	Indexing variable
mix	Flow mixer
mot	Electric motor
n	Nozzle
out	Total output from a component
pt	Power turbine
$static$	Static component
tot	Total

Chapter 1

Introduction

Numerous initiatives have been started for the aviation sector to reach net-zero carbon emissions by the year 2050 [1]–[3]. To that end, the International Air Transport Association (IATA) suggest in their Waypoint 2050 report that between 10% and 34% of the emissions reductions could come from improvements to aviation technology [4]. The United States Federal Aviation Administration (FAA) corroborates the lower bound of this range in their 2021 United States Aviation Climate Action Plan [5], where they estimate 10% of the total reductions will come from emergent technology. Waypoint 2050 calls out novel propulsion system architectures, such as fully or hybrid-electric aircraft in particular as promising improvement pathways, which some studies have supported. A selection of studies summarized in Table 1.1 of future conceptual hybrid-electric powertrains found fuel burn and nitrogen oxide emissions index (EI(NO_x)) benefits on the 2030 to 2050 time horizon of up to 10% and 4.9%, respectively.

If these new systems are going to become viable from a technological and economic perspective, tools will be needed to compare the performance of modern conventional and novel architectures. One such non-dimensional quantity is efficiency. In particular, the propulsion industry most commonly uses three primary terms to represent the efficiency of modern engines: overall, propulsive, and thermal efficiency [13], defined as

$$\eta_0 = \frac{\text{Thrust Power}}{\text{Fuel Power}} \tag{1.1}$$

Table 1.1: Selection of hybrid-electric engine percent metric improvements.

Study	Range [nmi]	Battery Specific Energy, E^* [Wh/kg]	ΔFuel [%]	ΔEI(NO_x) [%]
Lents et al. (2016) [6]	900	1000	−5.0	–
Seitz et al. (2018) [7]	500	1500	−6.6	–
Hoogreef et al. (2019) [8]	1100	500	−10.0	–
Lammen and Vankan (2020) [9]	1500	500	−6.0	−1.5
van Holsteijn et al. (2020) [10]	540	600	−1.8	–
Vouros et al. (2021) [11]	525	2000	–	−4.94
Kang et al. (2022) [12]	1000	1000	−2.5	−3.6

$$\eta_p = \frac{\text{Thrust Power}}{\text{Net Kinetic Energy Flow Across Engine}} \tag{1.2}$$

$$\eta_{th} = \frac{\text{Net Kinetic Energy Flow Across Engine}}{\text{Fuel Power}} \tag{1.3}$$

The overall efficiency can be decomposed into a product of thermal and propulsive efficiency, which represent the thermodynamic efficiency of the engine and how effectively the kinetic energy generated by the engine is converted to thrust, respectively. These three terms, alongside understanding of component isentropic and polytropic efficiencies [14], have been sufficient to characterize high level performance of modern turbofan engines. However, with novel engine architectures like hybrid-electrics beginning to be seriously considered by the aviation industry, we must ask whether these models are sufficient to capture their performance. Hybrid-electric engines add new powertrains (batteries and electric motors) independent of turbomachinery. The introduction of new energy storage mediums and non-turbomachinery components means the pure thermodynamic representation has little meaning.

Existing work has labeled the thermal efficiency equivalent for novel architectures inner efficiency, η_{in} [15]. However, this single term still fails to capture the intricacies of energy flow in these increasingly complex power systems. Numerous studies looking at novel architectures have defined efficiency expressions unique to a given configuration. These high-level models attempt to simply capture the energy flow of unconventional propulsion, but as a result do not define quantities equivalently to the models used in other systems, making comparison

difficult. Others have attempted to create scalable efficiency models for general architectures, however these scalable models either fail to capture energy flow pathways or fail to account for some steps in cross-stream energy flow. Examples of both types are presented in the following sections, along with the merits and drawbacks of their use. In particular, we focus here on the most commonly discussed of the novel architectures, hybrid-electrics.

1.1 Existing efficiency models in current analyses of novel architectures

1.1.1 High-level models

The most common high-level efficiency model is the inner/propulsive one widely used for conventional analysis today. As previously stated, this is sufficient for current engines, but lacks specificity as the number of power sources or complexity of components increases. Here we examine two representative examples of three-term models and discuss their benefits and deficiencies. The first of these models has been defined by Gladin et al. [16] for two-spool turbofans, consisting of core thermal efficiency, transmission efficiency, and propulsive efficiency, where core thermal and transmission efficiency are defined as:

$$\eta_{th,core} = \frac{\text{Net Kinetic Energy Flow Across Core}}{\text{Fuel Power}} \tag{1.4}$$

$$\eta_{tr} = \frac{\text{Net Kinetic Energy Flow Across Engine}}{\text{Net Kinetic Energy Flow Across Core}} \tag{1.5}$$

Combining these, overall efficiency is expressed as

$$\eta_0 = \eta_p \eta_{tr} \eta_{th,core} \tag{1.6}$$

While propulsive efficiency is identical to the 2-term case, the separation of thermal efficiency into a core and transmission term allows for distinct views of how effectively the fuel is being initially converted to useful energy and how effectively that energy is being transferred to

the exhaust jets of the engine. In an ultra-high bypass engine, the former would measure improvements to burner and thermodynamic performance, while the latter would measure improvements to the power transfer chain between the core and the propulsive fan.

Gladin et al. also extended this concept to hybrid electrics, adding the electric source power directly to the transmission efficiency:

$$\eta_{tr} = \frac{\text{Net Kinetic Energy Flow Across Engine}}{\text{Net Kinetic Energy Flow Across Core} + \text{Electrical Power}} \tag{1.7}$$

While Equation 1.7 does bookkeep electrical power, the details of some processes are lost. In particular, the mixing of electrical and kinetic power terms means the electrical powertrain is not evaluated separately, precluding comparison with a conventional equivalent. The inclusion of a source power in the denominator of a kinetic energy flow ratio means the term will be artificially deflated as the electrical source power will be higher than the kinetic power it is responsible for. As such, while this model is successful at separating thermodynamic, transmission, and propulsive efficiency for conventional engines, the inclusion of additional power sources prevents direct comparison between systems.

Another three term model is presented by Seitz et al. specifically to represent multi-power-source engines [17] [7]. This model consists of propulsive, transmission, and energy conversion efficiencies. Propulsive efficiency is again identical to the previous examples, with transmission and energy conversion efficiency being defined as:

$$\eta_{tr} = \frac{\text{Net Kinetic Energy Flow Across Engine}}{\text{Useful Power Generated from Supply Power}} \tag{1.8}$$

$$\eta_{th} = \frac{\text{Useful Power Generated from Supply Power}}{\text{Supply Power}} \tag{1.9}$$

While this model is similar to the Gladin's, there are differences that make the Seitz model more robust for multi-power-source systems. Namely, transmission efficiency uses useful power as a metric instead of a sum of kinetic and supply power. The energy conversion efficiency is allowed to be a catch-all term to capture the distinct processes which convert supply (e.g. carbon fuel, battery) power to useful power. In a hybrid system, the

energy conversion term is composed of a weighted sum of both fuel powertrain and battery powertrain efficiency chains. While this model does resolve the power type conflict from the Galdin model, this weighted sum introduces a new issue. It offers a more concise view of performance in exchange for losing information on how the powertrains affect each other.

Overall, these examples of high-level efficiency models succeed in giving a concise overview of where losses are occurring in complex propulsion systems, which may be desired for extremely quick iteration. To make best use of these models, a thorough understanding of the actual energy flow and what is not captured by the models is required. Without this understanding, the behavior of these terms may be harder to interpret. In exchange for concise representation, high-level models compromise on specific detail, failing to capture the exact energy flow. An improved model should thus be able to capture exact conversion pathways while being able to be simplified to a concise form.

1.1.2 Scalable models

Two primary forms of scalable efficiency models are seen in the existing literature: powertrain-based and exergy-based. The first of these, presented by Nam et al. [18], models a general propulsive system with n energy sources as n individual powertrains that act independently to generate propulsive power which can then be converted to thrust. Each powertrain is modeled as a product of efficiencies representing the specific conversion processes ocurring between the source power and the propulsive power. Example powertrain efficiency chains for conventional, battery, and fuel cell engines are presented by Hepperle [19]. While this approach is easily scalable to an arbitrary number of power sources, it lacks the ability to examine the interactions between individual power sources during conversion.

An exergy-based representation, presented by Schmitz and Hornung [15] expands inner efficiency as a sum of per-component availability losses. This approach could be scaled to any number of components in an engine, allowing for an exact representation of of arbitrarily complex systems. However, the summation used in this model removes any representation of energy flow in the system. While the component loss representation is useful, we still lack a model capturing the exact energy flow within propulsion systems.

1.2 Objective statement

Based on the review of existing efficiency models, we identify several traits required of a useful new efficiency model:

- The model must capture exact energy conversion pathways and interdependency of power sources at the component-by-component level.
- The full efficiency expression must be able to be condensed to a concise, easy to understand form (similar to 2 or 3-term models).
- Individual component losses must be extractable from the efficiency expression.

To that end, we create and demonstrate the use of a new generalized efficiency modelling system, called the Modular Efficiency Model (MEM). To demonstrate the model unmixed, mixed-flow, and hybrid-electric propulsion systems are numerically sized and have their performance compared using MEM metrics. Based on these comparisons, we identify applications where each examined architecture has the greatest potential benefits.

Chapter 2

Methods

In this work, we present the "Modular Efficiency Modeling" framework (MEM), a generalized system for defining component-wise efficiency of arbitrary propulsion systems in a way that is algebraically consistent and preserves representations of energy flow pathways. We first discuss the theory required for tracking power flow in a propulsive system. This is followed by an explanation of MEM itself, including the procedure used to assemble efficiency expressions. Finally, to demonstrate the use and applications of MEM, numerical simulation is performed on unmixed, mixed flow, and hybrid-electric architectures using the Numerical Propulsion System Simulation [20]. MEM is then used to identify key applications of novel technology, areas for improvement, and sizing criteria.

2.1 Power and energy flow characterization

To characterize propulsion system efficiency on a component level, several new quantities must be defined. We first introduce a metric for tracking the maximum useful kinetic energy flow in a stream at any point in the propulsion system, called expanded flow power (σ). We then present power degrees of hybridization (H_p), which are used to characterize the fraction of total system power supplied by one source.

2.1.1 Expanded flow power

Consider an ideal two-spool turbojet operating with the cycle shown in Figure 2.1. The useful mass-specific kinetic energy flow produced by this cycle is commonly defined as

$$\frac{\Delta KE}{\dot{m}} = \frac{u_9^2}{2} - \frac{u_0^2}{2} \tag{2.1}$$

This definition is composed of two terms. The first is the specific kinetic energy flow leaving the engine through the nozzle. The second is the freestream specific kinetic energy flow ingested by the engine. The difference in these terms represents the useful power generated by the engine. Each of these can be rewritten using the definition of stagnation enthalpy as

$$\frac{u^2}{2} = h_t - h \tag{2.2}$$

For the output flow, the stagnation enthalpy is the enthalpy at station 5. This flow is then expanded isentropically until it has static enthalpy equal to the value at station 9. A similar relation is true for the incoming flow with stations 2 and 0, respectively.

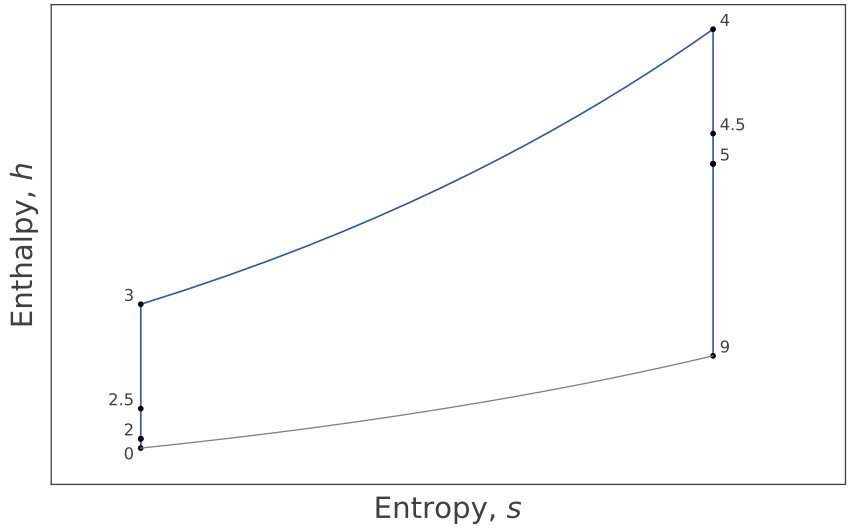

Figure 2.1: $h - s$ representation of an ideal 2-spool turbojet cycle.

Critically, this process assumes the flow is ideally expanded in the nozzle, such that

$$p_9 = p_0 \equiv p_{amb} \tag{2.3}$$

This condition also provides a practical maximum for the available propulsive energy. Further overexpansion of the nozzle flow would decrease thrust via suction while underexpansion would decrease the available kinetic energy flow rate. Knowing this, the concept can be extended to any point in a propulsion system as long as the ambient operating pressure is known. The expanded flow power at a point, ℓ, in a propulsion system is defined as the kinetic energy flow rate a stream would have if expanded to ambient pressure isentropically. Given a flow with known stagnation enthalpy and mass flow, the expanded flow power for a given ambient pressure, p_0, is:

$$\sigma_\ell = \dot{m}_\ell \Big(h_{t,\ell} - h_\ell \big|_{p=p_0} \Big) \tag{2.4}$$

In addition, the rise in expanded flow power between two points (ℓ_1, ℓ_2) can be defined as

$$\Delta\sigma_{\ell_2-\ell_1} = \sigma_{\ell_2} - \sigma_{\ell_1} \tag{2.5}$$

$\Delta\sigma$ terms will always be defined as downstream expanded flow power minus upstream expanded flow power for consistency. Mass-specific versions of these quantities can also be defined:

$$\hat{\sigma}_\ell = h_{t,\ell} - h_\ell \big|_{p=p_0} \tag{2.6}$$

$$\Delta\hat{\sigma}_{\ell_2-\ell_1} = \hat{\sigma}_{\ell_2} - \hat{\sigma}_{\ell_1} \tag{2.7}$$

Examples of these quantities are shown in Figure 2.2 below for an non-ideal turbojet. Note that the expanded flow power at station 4 goes from h_4 to the ambient pressure isobar, not h_9.

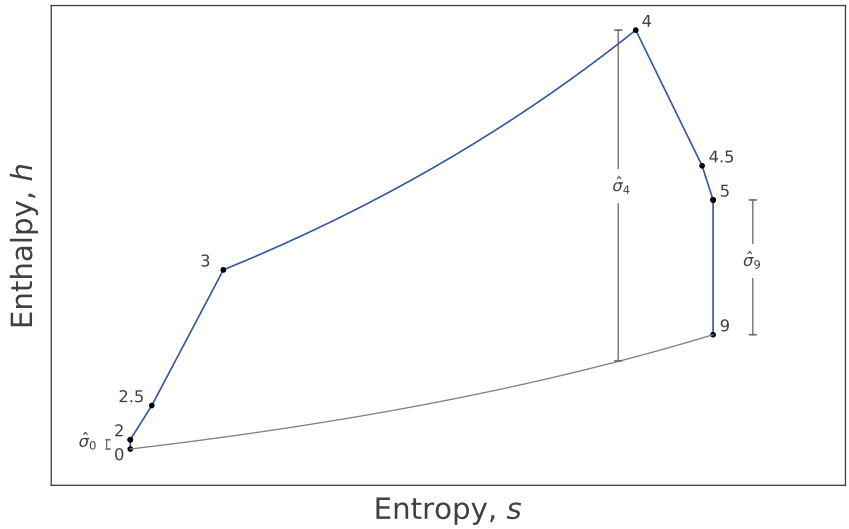

Figure 2.2: $h - s$ diagram representation of expanded flow power.

2.1.2 Degrees of power hybridization

While conventional air-breathing engines are powered by a single fuel, advanced concepts may introduce multiple power sources to the system. In the hybrid-electric case there would be both fuel and battery power. It is often desired to examine the fraction of total power supplied by one source. A metric used for fuel/battery systems is the degree of power hybridization [21], defined as

$$H_p = \frac{P_{bat}}{P_{bat} + P_f} \tag{2.8}$$

which quantifies how much of the source power is drawn from batteries at any given time. However, arbitrary systems could have more than two sources of many different types. As such, it is necessary to generalize this concept to n power sources $\left(P_{tot} = \sum_{i=1}^{n} P_i\right)$.

To do this, consider the contribution of the i^{th} power source, P_i/P_{tot}. This quantity is the i^{th} simple degree of power hybridization

$$H_p^i = \frac{P_i}{P_{tot}} \tag{2.9}$$

with the property that

$$\sum_{i=1}^{n} H_p^i = 1 \tag{2.10}$$

When discussing system efficiency, certain components are able to accept multiple sources of power as input. This results in efficiency expressions involving sums of simple degrees of power hybridization. For conciseness and clarity, the sum of H_p^i contributing to a component c^* is a composite degree of power hybridization, notated $H_p^{c^*}$.

As an example, consider a gas generator powered by Jet-A (P_{f1}) and hydrogen (P_{f2}) in multiple combustors. This gas generator is part of a larger system with $P_{tot} > P_{f1} + P_{f2}$. The gas generator degree of power hybridization would be:

$$H_p^{gg} = \frac{P_{f1} + P_{f2}}{P_{tot}} \tag{2.11}$$

This would also apply to a hybrid-electric system where the gas generator is powered by fuel and the electric motor is powered by a battery. In this case, the gas generator degree of power hybridization would be:

$$H_p^{gg} = \frac{P_f}{P_{tot}} \tag{2.12}$$

2.2 Efficiency assembly procedure

We have developed a framework using expanded flow power for assigning expressions for overall efficiency to arbitrarily complex air-breathing propulsion systems. These models consist of individual component efficiencies defined consistently between systems. This consistency allows for meaningful performance comparison of conventional and advanced propulsion system architectures. In addition, the component-by-component view allows for more detailed comparison of component efficiencies in a given system than existing models (e.g. thermal/propulsive efficiency for a turbofan).

Two terms are assumed to be defined for any architecture: overall and propulsive efficiency [13]. For an engine with n source powers, $P_i \mid i \,\epsilon\, [0, ..., n-1]$, the overall efficiency is

defined as thrust power ($F_n V_0$) divided by the total source power ($P_{tot} = \sum_{i=0}^{n-1} P_i$):

$$\eta_0 = \frac{F_n V_0}{P_{tot}} \tag{2.13}$$

Examples of power sources include, but are not limited to, fuels (Jet-A, hydrogen, etc.) and battery power. The propulsive efficiency measures how efficiently the useful energy produced by the engine is converted to thrust power in flight:

$$\eta_p = \frac{F_n V_0}{\text{Useful Kinetic Energy Flow}} \tag{2.14}$$

In Section 2.1.1, we defined the useful kinetic energy flow produced by a turbojet in terms of expanded flow power as $\Delta\sigma_{9-0}$. In general, propulsion systems can have multiple streams (e.g. core and bypass flow in a turbofan). For an engine with m streams, the total useful energy is is the sum of the useful energy produced in each stream. In general, an engine with m streams will have total expanded flow power rise, $\Delta\sigma_{tot}$, equal to

$$\Delta\sigma_{tot} = \sum_{j=0}^{m-1} \Delta\sigma_{j9-j0} \tag{2.15}$$

where $j9$ and $j0$ indicate the nozzle exit and freestream stations of the j^{th} stream, respectively. The first stream ($j = 0$) is denoted without a leading zero for consistency with the usual convention for turbofan engines. Propulsive efficiency is then written as:

$$\eta_p = \frac{F_n V_0}{\Delta\sigma_{tot}} \tag{2.16}$$

If overall efficiency is written as a function of propulsive efficiency, a term ($\Delta\sigma_{tot}/P_{tot}$) emerges. Expanding this term as a sum of each stream's expanded flow power rise, the overall efficiency for a given architecture is:

$$\eta_0 = \eta_p \left[\frac{\Delta\sigma_{9-0}}{P_{tot}} + \frac{\Delta\sigma_{19-10}}{P_{tot}} + ... + \frac{\Delta\sigma_{(m-1)9-(m-1)0}}{P_{tot}} \right] \tag{2.17}$$

While the bracketed terms are ratios of powers, they are not efficiencies. Each term represents

a fraction of the total expanded flow power rise generated from the total source power. Non-efficiency ratios of power are designated in this work as power fractions (ϵ). In general, the power fraction between two stations is notated similarly to rise in expanded flow power, with a $i-j$ subscript:

$$\epsilon_{i-j} = \frac{\Delta\sigma_{i-j}}{P_{tot}} \tag{2.18}$$

The particular case of the freestream-to-nozzle power fractions occur frequently and are called stream power fractions. These are notated by

$$\epsilon_j^{st} = \frac{\Delta\sigma_{j9-j0}}{P_{tot}} \tag{2.19}$$

With this, the overall efficiency is written as

$$\eta_0 = \eta_p\left[\epsilon_0^{st} + \epsilon_1^{st} + ... + \epsilon_{m-1}^{st}\right] \tag{2.20}$$

Note that while the stream power fraction for stream 0 still includes the zero in the notation, the expanded expression (containing $\Delta\sigma_{9-0}$) does not. This is due to the difference in using station numbering versus streamwise numbering. The expanded flow power terms are labeled using station numbers where we drop leading zeros. The stream power fractions are notated using the index of the associated stream.

Once in this form, unique expressions for each stream power fraction must be determined. These expressions will depend on the specific components affecting the flow in a given stream, such as fans, gas generators, or ducts. Each component in a propulsion system has flow power metrics - most commonly efficiency - that quantify its performance. A complete stream power fraction expression will be a function purely composed of component flow power performance metrics and degrees of power hybridization. Thus, to construct a stream power fraction, we need to know three primary pieces of information for each component:

1. Definitions of all flow power metrics for a given component.
2. How to combine flow power metrics to accurately represent energy flow in a system.
3. When and how to incorporate degrees of power hybridization.

Five primary categories of components have been identified which have common metric definitions and implementations: static components (e.g. nozzles), flow power producers (e.g. fans), flow power extractors (e.g. turbines), flow mixers, and bleeds (e.g. cooling flows). In addition, it is also possible to have components that do not directly influence the flow in a stream (e.g. gearboxes). This adds a sixth, non-flow, category. The following sections examine the three points above for each category.

2.2.1 Static components

Flow Power Efficiency and Degree of Power Hybridization Definitions

Static components have one flow input and one flow output. They are assumed to be adiabatic, have no shaft work, and dissipate some energy in the flow due to friction or other non-isentropic loss processes, as shown in Figure 2.3. Examples of static components include ducts, inlets, and nozzles. The flow power efficiency of a static component is defined as the ratio of output to input expanded flow power,

$$\eta_{static} = \frac{\sigma_{out}}{\sigma_{inp}} \tag{2.21}$$

Static components by definition do not accept input from a system power source. As such, they will never involve degrees of power hybridization.

Integration Into Larger Systems

Consider a system where a non-static component (A) is surrounded by a duct on the left (D_L) and a duct on the right (D_R), as shown with station numbers in Figure 2.4. The stream power fraction for this stream is

$$\epsilon_0^{st} = \frac{\Delta\sigma_{9-0}}{P_{tot}} \tag{2.22}$$

The left duct has efficiency $\eta_{D_L} = \sigma_2/\sigma_0$ and the right duct has efficiency $\eta_{D_R} = \sigma_9/\sigma_5$. Using these definitions, the stream power fraction can be written in terms of σ_5 and σ_2:

$$\epsilon_0^{st} = \frac{1}{P_{tot}}\left(\sigma_5\eta_{D_R} - \sigma_2\eta_{D_L}^{-1}\right) \tag{2.23}$$

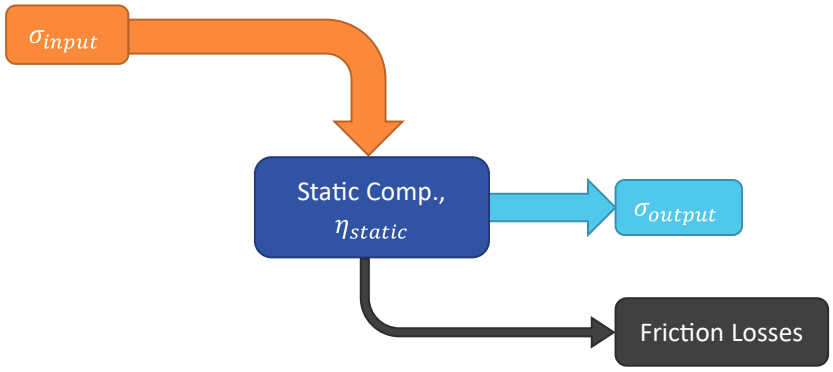

Figure 2.3: Energy flow in a static component.

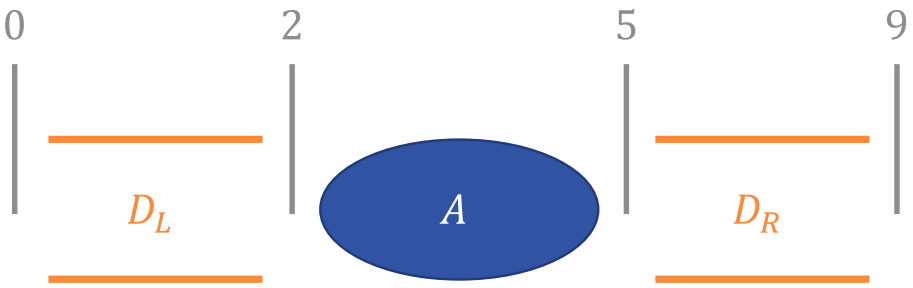

Figure 2.4: Stream with two static elements, D_L and D_R, surrounding component, A.

Note that the power fraction is assigned subscript $j = 0$ as this system only has one stream. By multiplying this expression by 1 in the form $\Delta\sigma_{5-2}/\Delta\sigma_{5-2}$, the stream power fraction becomes:

$$\epsilon_0^{st} = \frac{\sigma_5\eta_{D_R} - \sigma_2\eta_{D_L}^{-1}}{\Delta\sigma_{5-2}} \frac{\Delta\sigma_{5-2}}{P_{tot}} \tag{2.24}$$

The first term in this equation represents loss of expanded flow power rise generated by component A due to static losses on both the inlet and outlet sides. Terms of this form will appear often, and are notated more concisely using the static loss fraction, κ. In general, for a region of a stream bounded by static components where the stations at the outer bounds are i (downstream) and j (upstream), and the stations at the inner bounds of the static components are k (downstream) and ℓ (upstream), the associated static loss fraction

is defined as:

$$\kappa_{k-\ell}^{i-j} = \frac{\Delta\sigma_{i-j}}{\Delta\sigma_{k-\ell}} = \frac{\sigma_k \prod \eta_{downstream} - \sigma_\ell \prod \eta_{upstream}^{-1}}{\Delta\sigma_{k-\ell}} \tag{2.25}$$

In this case, as the numerator is $\Delta\sigma_{9-0}$ and the denominator is $\Delta\sigma_{5-2}$ with D_R and D_L as bounding elements, it is condensed to κ_{5-2}^{9-0}, making the stream power fraction:

$$\epsilon_0^{st} = \kappa_{5-2}^{9-0} \frac{\Delta\sigma_{5-2}}{P_{tot}} \tag{2.26}$$

The second term in Equation 2.26 is a measure of how efficiently A generates expanded flow power rise using system source power. If the system in question was a turbojet, A would represent a gas generator experiencing some inlet and nozzle losses.

This process can be repeated for internal ducts as well. Consider a system consisting of a duct (D_L), a non-static component (A_1), another duct (D_C), a second non-static component (A_2), and a final duct (D_R) with station numbering shown in Figure 2.5.

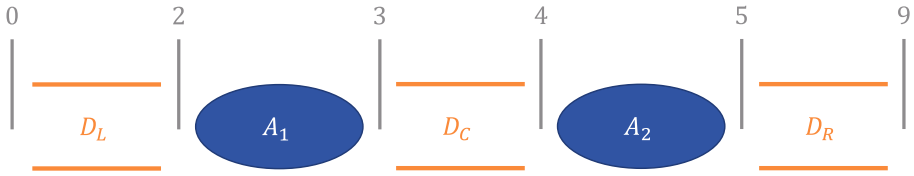

Figure 2.5: Two component groups (A_1, A_2) separated by static elements.

The stream power fraction of this system can be split into two subsystems:

$$\epsilon_0^{st} = \frac{\Delta\sigma_{9-4}}{P_{tot}} + \frac{\Delta\sigma_{4-0}}{P_{tot}} \tag{2.27}$$

The first term in Equation 2.27 represents the system consisting of A_2 and D_R. The second term represents the system consisting of D_L, A_1, and D_C. Each of these terms represent an arbitrary collection of components surrounded by static elements. In the first term, there is no upstream component, which is effectively equivalent to having an ideal static element. As such, both of these terms can be written in the form derived for the prior case, yielding:

$$\epsilon_0^{st} = \frac{\sigma_5 \eta_{D_R} - \sigma_4}{\Delta\sigma_{5-4}} \frac{\Delta\sigma_{5-4}}{P_{tot}} + \frac{\sigma_3 \eta_{D_C} - \sigma_2 \eta_{D_L}^{-1}}{\Delta\sigma_{3-2}} \frac{\Delta\sigma_{3-2}}{P_{tot}} \tag{2.28}$$

Using static loss fractions, this condenses to:

$$\epsilon_0^{st} = \kappa_{5-4}^{9-4}\frac{\Delta\sigma_{5-4}}{P_{tot}} + \kappa_{3-2}^{4-0}\frac{\Delta\sigma_{3-2}}{P_{tot}} \tag{2.29}$$

2.2.2 Flow power producers

Flow Power Efficiency and Degree of Power Hybridization Definitions

Flow power producers can consume a combination of system source powers and shaft powers to increase the expanded flow power in a stream, as shown in Figure 2.6. Examples of

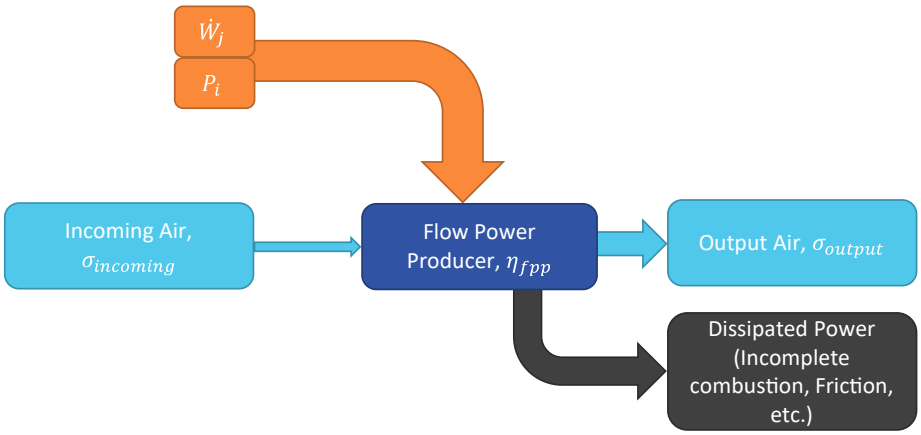

Figure 2.6: Energy flow in a flow power producer.

flow power producers include gas generators and fans. The number and type of inputs is determined by component design. For example, gas generators typically receive input from a fuel source while fans are powered by a single shaft input. Assuming the expanded flow power rise across a flow power producer powered by n system source powers and m shafts is $\Delta\sigma_{out-inp}$, the component's efficiency is defined as

$$\eta_{fpp} = \frac{\Delta\sigma_{out-inp}}{\sum_{i=0}^{n-1} P_i + \sum_{j=0}^{m-1} \dot{W}_i} \tag{2.30}$$

For any flow power producer, there will be an associated power usage term of the form:

$$\left[\frac{\sum_{i=0}^{n-1} P_i + \sum_{j=0}^{m-1} \dot{W}_i}{P_{tot}}\right]$$

The ratios $\sum_i P_i/P_{tot}$ represents a sum of degrees of power hybridization, $\sum_i H_{p,i}$. The other term take the form $\sum_j \dot{W}_j/P_{tot}$. These are not degrees of power hybridization. Ratios of shaft power and total source power of this form are called shaft power fractions (ϵ^{sh}). By following the shaft power to its source (e.g. power turbine, electric motor, etc.), shaft power fractions can be written as functions of degrees of power hybridization as well. As such, the ratio $\Delta\sigma_{out-inp}/P_{tot}$ can be written as:

$$\frac{\Delta\sigma_{out-inp}}{P_{tot}} = \eta_{fpp}\left[\sum_{i=0}^{n-1} H_{p,i} + \sum_{j=0}^{m-1} \epsilon_j^{sh}\right] \tag{2.31}$$

Integration Into Larger Systems

Consider the system shown previously in Figure 2.4, where we now assume that component A is a flow power producer. From the discussion of static components, the stream power fraction of this system is

$$\epsilon_0^{st} = \kappa_{5-2}^{9-0}\frac{\Delta\sigma_{5-2}}{P_{tot}} \tag{2.32}$$

The flow power producer, A, generates $\Delta\sigma_{out-inp} = \Delta\sigma_{5-2}$ given source power, P_A, such that $\eta_A = \Delta\sigma_{5-2}/P_A$. Equation 2.32 can then be written in terms of η_A and the power hybridization:

$$\epsilon_0^{st} = \kappa_{5-2}^{9-0}\eta_A H_p^A \tag{2.33}$$

The composite degree of power hybridization for component A is used here for conciseness. In the case of multiple flow power producers in series, the contributions to the net expanded flow power rise will combine additively. Consider an equivalent example where A is split into two flow power producers, A_1 and A_2, each with a single source power input. The stream power fraction becomes:

$$\epsilon_0^{st} = \kappa_{5-2}^{9-0}\left(\eta_{A_1} H_p^{A_1} + \eta_{A_2} H_p^{A_2}\right) \tag{2.34}$$

2.2.3 Flow power extractors

Flow Power Efficiency and Degree of Power Hybridization Definitions

Flow power extractors are components that extract some fraction of an incoming flow power rise ($\Delta\sigma_{inp}$) produced by one or more upstream flow producers. The extracted flow power ($\Delta\sigma_{ext}$), equal to the drop in expanded flow power across the component, is then delivered to another component or stream in the system. They are characterized by two primary parameters: the extraction fraction, E_p, and the component flow power efficiency, η_{ext}. The former is defined as the expanded flow power extracted from the stream over the incoming rise in expanded flow power,

$$E_p = \frac{-\Delta\sigma_{ext}}{\Delta\sigma_{inp}} \tag{2.35}$$

The negative of the extracted power drop is used as $\Delta\sigma_{ext}$ is negative as flow power is removed from the flow across the component. After the extractor, a fraction $(1 - E_p)$ of the incoming expanded flow power rise will remain in the stream.

The flow power efficiency for a flow power extractor is dependent on what is done with the extracted energy. It could be converted to shaft power as in a turbine, converted directly to flow power in another stream as in a heat exchanger, or it could undergo another process. Regardless, the extractor efficiency will take the form

$$\eta_{ext} = \frac{[\text{output}]}{-\Delta\sigma_{ext}} \tag{2.36}$$

where the output term is replaced with the appropriate component output. The energy flow in a flow power extractor is shown in Figure 2.7. Based on these terms, the expressions representing rejected flow power rise and output power purely in terms of input flow power rise are

$$\frac{\Delta\sigma_{rejected}}{P_{tot}} = (1 - E_p)\frac{\Delta\sigma_{inp}}{P_{tot}} \tag{2.37}$$

$$\frac{[\text{output}]}{P_{tot}} = \eta_{ext}E_p\frac{\Delta\sigma_{inp}}{P_{tot}} \tag{2.38}$$

Assuming the input expanded flow power rise is generated by one or more upstream flow

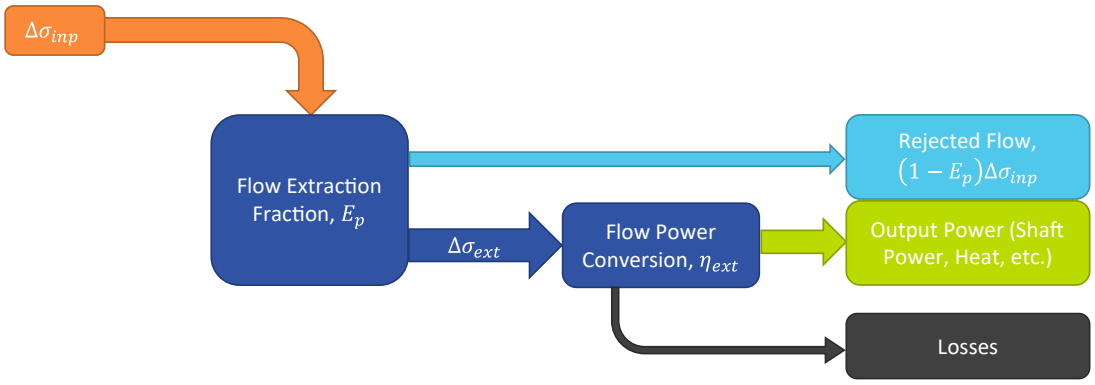

Figure 2.7: Energy flow in a flow power extractor.

power producers, the $\Delta\sigma_{inp}/P_{tot}$ term can be written in terms of the efficiency and degrees of power hybridization of those producers.

Integration Into Larger Systems

Consider a system consisting of up/downstream ducts (D_L and D_R), a flow power producer (A), and a power turbine (Trb) as shown with station numbers in Figure 2.8. The stream power fraction can be split similarly to the series flow producers case in the previous section:

$$\epsilon_0^{st} = \kappa_{5-2}^{9-0}\left(\frac{\Delta\sigma_{4.7-2} + \Delta\sigma_{5-4.7}}{P_{tot}}\right) \tag{2.39}$$

Here, $\Delta\sigma_{4.7-2}$ is the rise in expanded flow power across A. As such, the first term in Equation 2.39 can be simplified using flow producer efficiency:

$$\epsilon_0^{st} = \kappa_{5-2}^{9-0}\left(\eta_A H_p^A + \frac{\Delta\sigma_{5-4.7}}{P_{tot}}\right) \tag{2.40}$$

In this case, $\Delta\sigma_{ext} = \Delta\sigma_{5-4.7}$. The rise in expanded flow power entering the power turbine is the rise across the gas generator, $\Delta\sigma_{inp} = \Delta\sigma_{4.7-2}$. Knowing this, the stream power fraction is written as:

$$\epsilon_0^{st} = \kappa_{5-2}^{9-0}\left(\eta_A H_p^A - E_p\frac{\Delta\sigma_{4.7-2}}{P_{tot}}\right) \tag{2.41}$$

Using the definition of flow producer efficiency, Equation 2.41 reduces to the fraction of expanded flow power rise rejected to the stream $(1 - E_p)$ multiplied by the gas generator efficiency and degree of hybridization:

$$\epsilon_0^{st} = \kappa_{5-2}^{9-0}\left(\eta_A H_p^A - E_p \eta_A H_p^A\right) \tag{2.42}$$

$$\epsilon_0^{st} = \kappa_{5-2}^{9-0}(1 - E_p)\eta_A H_p^A \tag{2.43}$$

The shaft power produced by the power turbine must now be accounted for elsewhere in the propulsion system. In this case, it is assumed that the shaft power ($\epsilon^{sh} = \eta_{pt} E_p \eta_A H_p^A$) is used to power a flow producer in a second stream.

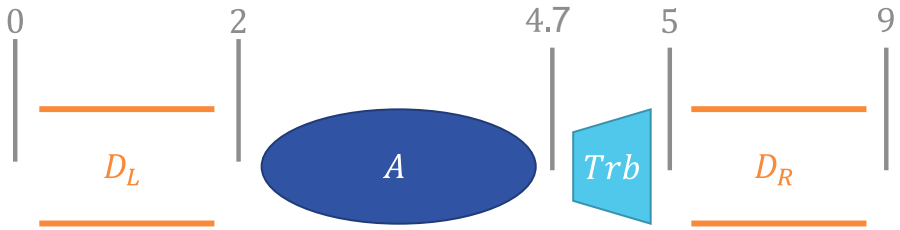

Figure 2.8: Example of a propulsive stream with a power turbine extracting flow power.

2.2.4 Flow mixers

Flow Power Efficiency and Degree of Power Hybridization Definitions

Flow mixers are adiabatic components with no shaft work that take s stream inputs and mixes them into one output stream. Some exergy is dissipated in the mixing process. A well-designed flow mixer accepting streams of differing stagnation enthalpy acts to increase the thrust of the system compared to an unmixed equivalent. As mass is conserved while mixing, this means that the jet velocity of the mixed stream will be greater than the mass-averaged jet velocity of the individual streams. As defined in Section 2.1.1, the expanded flow power is a measure of maximum propulsive kinetic energy flow, and is proportional to u^2. As we can obtain an output flow power larger than the input flow powers, we choose to

characterize mixers not with efficiency, but with effectiveness:

$$\chi_{mix} = \frac{\sigma_{out}}{\sum_{i=0}^{s-1} \sigma_{inp,i}} \tag{2.44}$$

This quantity can be greater than one. While the flow power can increase across a mixer, the total useful energy of the flow, characterized by exergy, always decreases. For more details on flow power and its relation to exergy, see Appendix B. Similar to static components, mixers do not accept any source or shaft power, so no degrees of power hybridization appear.

Integration Into Larger Systems

Consider a two stream system ($m \, \epsilon \, [0, 1]$) with a mixer. The output stream (and all stations post-mixer) are notated with the lowest stream number (in this case, $m = 0$). An example of this system and station numbering is shown in Figure 2.9. The stream power fraction across the entire system is

$$\epsilon_0^{st} = \frac{\sigma_9 - (\sigma_0 + \sigma_{10})}{P_{tot}} \tag{2.45}$$

The mixer effectiveness for this system is

$$\chi_{mix} = \frac{\sigma_7}{\sigma_6 + \sigma_{16}} \tag{2.46}$$

Assuming the nozzle has efficiency, $\eta_n = \sigma_9/\sigma_7$, and other components are ideal, the stream power fraction becomes

$$\epsilon_0^{st} = \frac{(\sigma_6 + \sigma_{16})\chi_{mix}\eta_n - (\sigma_0 + \sigma_{10})}{P_{tot}} \tag{2.47}$$

Multiplying by 1 in the form $\frac{\Delta\sigma_{6-0}+\Delta\sigma_{16-10}}{\Delta\sigma_{6-0}+\Delta\sigma_{16-10}}$,

$$\epsilon_0^{st} = \frac{(\sigma_6 + \sigma_{16})\chi_{mix}\eta_n - (\sigma_0 + \sigma_{10})}{\Delta\sigma_{6-0} + \Delta\sigma_{16-10}} \frac{\Delta\sigma_{6-0} + \Delta\sigma_{16-10}}{P_{tot}} \tag{2.48}$$

The second term in Equation 2.48 is the sum of the individual stream power fractions (up to the mixer) of both mixed streams. Stream power fractions of this form are notated $\epsilon_{j,mix}^{st}$. In addition, we introduce an augmented form of the static loss fraction, κ, for cases where flows mix directly in one stream. If there are multiple inputs or outputs being accounted

for, we separate the shared inputs and outputs in the notation with a comma. In this case, there is one output stream exiting at station 9 and two input streams at stations 0 and 10. The output stream is generated by mixing two input streams at stations 6 and 16. As such, the static loss fraction for this system is:

$$\kappa_{6,16-0,10}^{9-0,10} = \frac{\sigma_9 - (\sigma_0 + \sigma_{10})}{\Delta\sigma_{6-0} + \Delta\sigma_{16-10}} \tag{2.49}$$

Using this and substituting in a static loss fraction, the overall stream power fraction is:

$$\epsilon_0^{st} = \kappa_{6,16-0,10}^{9-0,10}\left(\epsilon_{0,mix}^{st} + \epsilon_{1,mix}^{st}\right) \tag{2.50}$$

From here, the mixed stream power fractions can be determined using the procedures outlined in this section.

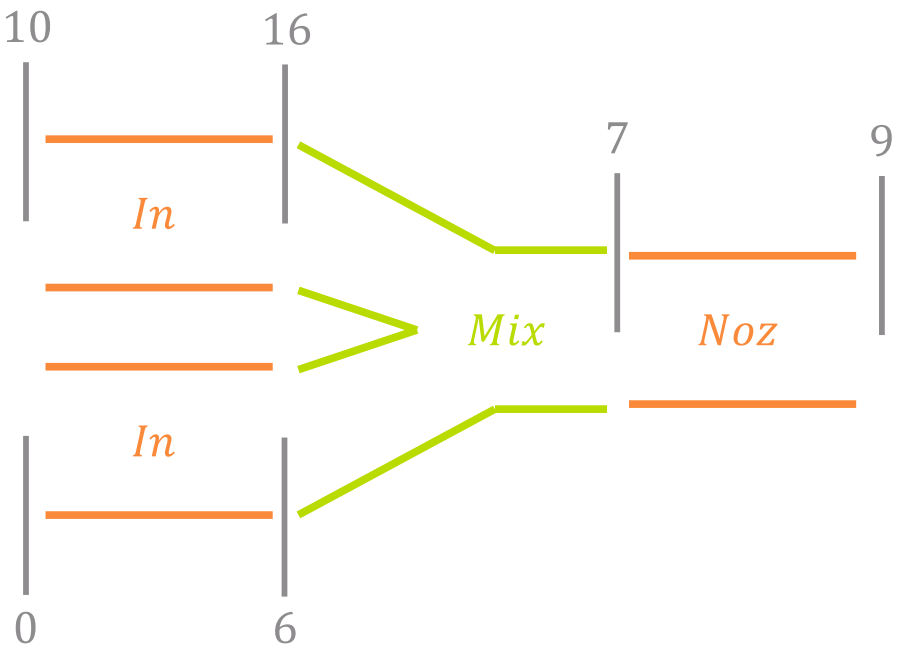

Figure 2.9: Example of a 2-stream mixed flow system.

2.2.5 Bleeds

Bleeds are adiabatic components which extract flow power from a stream by directly removing some mass of air. They accept one stream as an input and have two streams as outputs. As they do not have a source or shaft power input, they have no associated degree of power hybridization. Functionally, bleeds share similarities to flow power extractors, but have some key differences. The primary source of this difference is derived from the type of bleed being examined. The types of bleeds discussed in this work are cooling bleeds, overboard bleeds, and cross-stream leakage. The implementation of each type requires similar, but distinct, procedures. While the exact methods described here may not be applicable to bleed flows of other types, the same thought process can be used to determine their implementations. The following sections examine each identified bleed type individually.

Cooling bleeds

Cooling bleeds are isobarically extracted from an upstream component and re-injected in a downstream component as a form of active cooling. In such cases, the bleed flow is usually extracted and injected within non-isentropic components, not necessarily at the entrance or exit. There are two primary ways to handle these bleeds:

- Split the component receiving/giving the cooling flow into two sub-components with equal polytropic efficiency. Model the bleed as a component between the split turbomachine. Repeat this for as many bleed flows as are present in the component.
- Include the bleed flow(s) in the net flow power in/out of a component and integrate them directly into component efficiencies.

In this thesis, we consider only the second option for conciseness, but the first option should be investigated and modeled in future work.

Consider the system shown in Figure 2.10 where a gas generator (A) has some flow power bled off (σ_{bld}) to cool a power turbine (Trb).
While no independent bleed efficiency appears in the stream power fraction, two changes have to be made. The stream power fraction of the equivalent system with no bleed flows

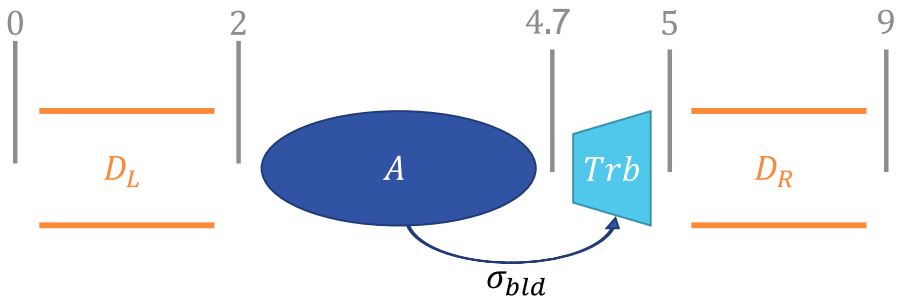

Figure 2.10: Example of a propulsive stream with a cooling bleed flow.

was

$$\epsilon_0^{st} = \kappa_{5-2}^{9-0}(1 - E_p)\eta_A H_p^A \tag{2.51}$$

where

$$\eta_A = \frac{\Delta\sigma_{4.7-2}}{P_A}, \qquad E_p = \frac{-\Delta\sigma_{5-4.7}}{\Delta\sigma_{4.7-2}}$$

The bleed flow introduces an additional flow power output to A and an additional input to Trb which must be accounted for in their respective $\Delta\sigma$ terms. To include the effect of the bleed flow, σ_{bld} is added to the output flow power of the gas generator and to the input flow power of the power turbine, such that

$$\eta_A = \frac{(\sigma_{4.7} + \sigma_{bld}) - \sigma_2}{P_A}, \qquad E_p = -\frac{\sigma_5 - (\sigma_{4.7} + \sigma_{bld})}{(\sigma_{4.7} + \sigma_{bld}) - \sigma_2}$$

Based on this definition, we expect cooling bleed flow power to be present only when it enters/exits a component's control volume separately from the primary flow. This implies that the cumulative expression for the gas generator and power turbine should not have a σ_{bld} term, as the cooling flow is entirely contained between those two components. The expression for the power fraction across both components is

$$\epsilon_{5-2} = (1 - E_p)\eta_A H_p^{gg} \tag{2.52}$$

Expanding this in terms of flow powers gives

$$\epsilon_{5-2} = \left(1 + \frac{\sigma_5 - (\sigma_{4.7} + \sigma_{bld})}{(\sigma_{4.7} + \sigma_{bld}) - \sigma_2}\right)\frac{(\sigma_{4.7} + \sigma_{bld}) - \sigma_2}{P_f} H_p^{gg} \tag{2.53}$$

Condensing the $1 - E_p$ term yields

$$\epsilon_{5-2} = \left(\frac{(\sigma_{4.7} + \sigma_{bld}) - \sigma_2 + \sigma_5 - (\sigma_{4.7} + \sigma_{bld})}{(\sigma_{4.7} + \sigma_{bld}) - \sigma_2} \right) \frac{(\sigma_{4.7} + \sigma_{bld}) - \sigma_2}{P_f} H_p^{gg} \tag{2.54}$$

The term $(\sigma_{4.7} + \sigma_{bld})$ fully cancels from the expression, leaving

$$\epsilon_{5-2} = \frac{\Delta\sigma_{5-2}}{P_{tot}} \tag{2.55}$$

which is the definition of the power fraction presented previously. In cases where the bleed flow takes a more complicated path, care must be taken to modify the component metrics appropriately.

Overboard bleeds

Like cooling bleeds, overboard bleeds isobarically extract mass from a flow. However, instead of being re-injected into the engine, the extracted flow is removed from the propulsion system for use elsewhere in an aircraft. As such, the source component metrics are modified identically to the cooling flow implementation. However, as the extracted flow never reenters the engine, it must be accounted for in all upstream components. Consider the system shown in Figure 2.11. The stream power fraction takes the form

$$\epsilon_0^{st} = \kappa_{5-2}^{9-0}(1 - E_p)\eta_A H_p^A \tag{2.56}$$

with

$$\eta_A = \frac{(\sigma_{4.7} + \sigma_{bld} - \sigma_2)}{P_f} \tag{2.57}$$

Unlike the cooling flow example, the bleed does not enter the turbine, leading to the turbine extraction fraction being

$$E_p = -\frac{\Delta\sigma_{5-4.7}}{(\sigma_{4.7} + \sigma_{bld} - \sigma_2)} \tag{2.58}$$

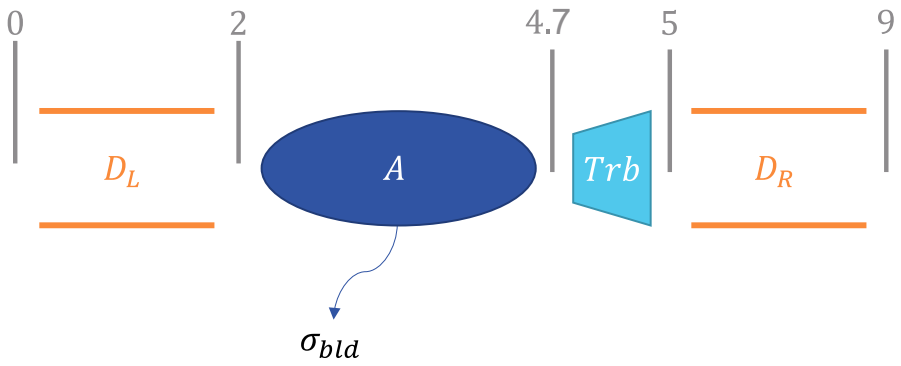

Figure 2.11: Example of a propulsive stream with an overboard bleed.

meaning that the power fraction from station 5 to station 2 would be

$$\epsilon_{5-2} = (1 - E_p)\eta_A H_p^A = \frac{(\sigma_5 + \sigma_{bld}) - \sigma_2}{P_{tot}} \tag{2.59}$$

To resolve the static loss fraction, κ_{5-2}^{9-0}, the bleed flow is treated as an output stream with no static losses such that

$$\kappa_{5-2}^{9-0} = \frac{(\eta_{D_R}\sigma_5 + \sigma_{bld}) - \eta_{D_L}^{-1}\sigma_2}{(\sigma_5 + \sigma_{bld}) - \sigma_2} \tag{2.60}$$

As a consequence of this accounting method, overboard flows lead to decreases in propulsive efficiency. We define propulsive efficiency as thrust power over the net flow power rise across the engine. The engine still utilizes source power to produce the bleed flow power, but does not convert it to thrust. By definition this indicates a lower propulsive efficiency. This is apparent if we look at the propulsive efficiency term:

$$\eta_p = \frac{F_N u_0}{(\sigma_9 + \sigma_{bld}) - \sigma_0} \tag{2.61}$$

Cross-stream leakage

Cross-stream leakage bleeds are standalone components that connect two streams, allowing a small amount of mass to pass between. They are nearly identical to a power turbine in function, with the exception that instead of converting flow power into shaft power, they directly transfer flow power from one stream to another. There are two primary parameters that characterize a leakage bleed. The first is an extraction fraction (B_p) representing the

fraction of the flow power isobarically extracted from the provider stream. The second is an effectiveness (χ), similar to that of a mixer, representing the flow power recovered or dissipated when the bleed flow mixes with the receiving stream. As was also the case for a mixer, the exergy of the receiving flow plus the bleed will never increase through this process.

For the sake of analysis, we define two points in the leakage bleed, shown in Figure 2.12. The first of these is $B_{1,out}$, representing the point where flow is extracted. Like the case of flow extractors, we assume the bleed flow is extracting a portion of the incoming rise in flow power produced by one or more upstream producers. In the example given, the incoming flow power rise is provided by A_2 ($\Delta\sigma_{A_2}$). The second, $B_{1,in}$, is the point where the bleed flow is mixed into the receiver stream. Knowing this, the bleed extraction fraction and bleed effectiveness are defined as

$$B_p = -\frac{\Delta\sigma_{B_{1,out}}}{\Delta\sigma_{A_2}} = -\frac{\Delta\sigma_{13.1-13}}{\Delta\sigma_{13-12}} \tag{2.62}$$

$$\chi_{bld} = -\frac{\Delta\sigma_{B_{1,in}}}{\Delta\sigma_{B_{1,out}}} = -\frac{\Delta\sigma_{5.1-5}}{\Delta\sigma_{13.1-13}} \tag{2.63}$$

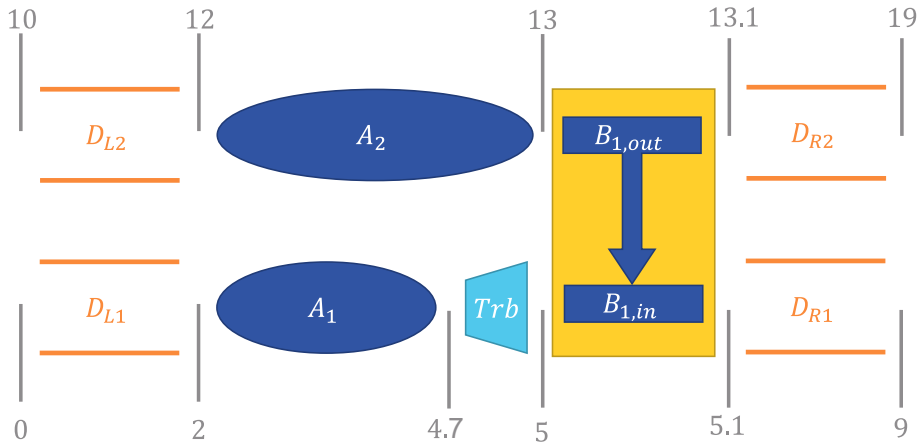

Figure 2.12: Example of a 2-stream system with a leakage bleed from stream 1 to stream 0.

Stream 0 without the bleed has a stream power fraction of

$$\epsilon_0^{st} = \kappa_{5.1-2}^{9-0}(1 - E_p)\eta_{A_1} H_p^{A_1} \tag{2.64}$$

However, as flow power is being added to stream 0 via the bleed between stations 5 and 5.1,

it is necessary to add $\Delta\sigma_{B_{1,in}}/P_{tot}$ to the flow power contributions. We assume here that A_2 is a fan powered by the shaft output of Trb. However, A_2 could be any number and type of flow producers, as long as a complete MEM expression can be formed for them. Using the metrics defined in this and all prior sections, the stream 0 power fraction for this example is

$$\epsilon_0^{st} = \kappa_{5.1-2}^{9-0}\left((1-E_p)\eta_{A_1}H_p^{A_1} + \chi_{bld}B_p\left[\eta_{A_2}\eta_{Trb}E_p\eta_{A_1}H_p^{A_1}\right]\right) \tag{2.65}$$

Stream 1 is characterized using a similar process, yielding

$$\epsilon_1^{st} = \kappa_{13.1-12}^{19-10}(1-B_p)\eta_{A_2}\eta_{Trb}E_p\eta_{A_1}H_p^{A_1} \tag{2.66}$$

2.2.6 Non-flow components

The final category of components are those that do not directly influence the flow in an engine. In particular, a non-flow component is one that does not depend directly on flow power. This is a broad enough category that it would be impossible to capture all such components here. As such, we present simple definitions of non-flow component efficiencies which are relevant to the work at hand. Two such components are of interest here: electric motors and mechanical differentials. We define the former as devices that produce shaft power given electrical power. The latter we define as devices that act to sum the shaft powers of n input shafts such that $\dot{W}_{out} \leq \sum_{i=0}^{n-1}\dot{W}_i$. Using these definitions, the efficiency of each device is as follows:

$$\eta_{mot} = \frac{\dot{W}}{P_{elec}} \tag{2.67}$$

$$\eta_{diff} = \frac{\dot{W}_{out}}{\sum_{i=0}^{n-1}\dot{W}_i} \tag{2.68}$$

Importantly, electrical power can be a source power for a propulsion system (e.g. batteries). As such, motors may have an associated simple or composite degree of power hybridization.

2.2.7 MEM expression assembly summary

An air-breathing propulsion system with n input power sources ($P_{tot} = \sum_{i=0}^{n-1} P_i$) and producing thrust power, $F_n u_0$, has overall efficiency [13]:

$$\eta_0 = \frac{F_n u_0}{P_{tot}} \tag{2.69}$$

For a system with m streams, this can always be expressed as a function of propulsive efficiency [13] $\left(\eta_p = \frac{F_n V_0}{\sum_{j=0}^{m-1} \Delta\sigma_{j9-j0}}\right)$ and a sum of stream power fractions:

$$\eta_0 = \eta_p \left[\epsilon_0^{st} + \epsilon_1^{st} + ... + \epsilon_{m-1}^{st}\right] \tag{2.70}$$

Each stream power fraction is determined by collections of components grouped into static components, flow power producers, flow power extractors, flow mixers, bleeds, and non-flow components. Using definitions of component performance metrics, overall efficiency can be expressed as a function of these metrics and degrees of power hybridization, such that

$$\eta_0 = f(H_p^i, \eta_i, \chi_i, E_p^i, ...) \tag{2.71}$$

2.3 Description of engine architectures and evaluation methods

To demonstrate the Modular Efficiency Model, five primary engine architectures are simulated in NPSS. Of these, three are based on the CFM56-7B cycle deck created by Lee et al. [22]. These subsonic architectures consist of an unmixed turbofan, a mixed-flow turbofan, and a hybrid-electric turbofan. The other two engines are based on the clean-sheet supersonic transport (SST) engine cycle deck created by Prashanth et al. [23]. The SST engine architectures consist of an unmixed turbofan and a mixed-flow turbofan. For analysis, we assume these variants are being retrofit onto appropriate aircraft with set baseline payload mass. We take the unmixed engines as baseline scenarios and then compare the mixed-flow and hybrid variants to these baseline cases in terms of MEM metrics, takeoff/climb fuel

Table 2.1: Selected mission points for subsonic and SST engine sizing.

	Subsonic				SST			
	t [min]	Alt [km]	Mach	F_N [kN]	t [min]	Alt [km]	Mach	F_N [kN]
SLS	0.0	0.0	0.0	91.46	0.0	0.0	0.0	73.9
TOC	37.0	10.7	0.76	27.1	52.1	12.5	1.40	24.0
CRZ	40.7	10.7	0.78	22.5	57.6	13.3	1.40	21.1

burn, and remaining payload mass. All engine variants are sized using multi-design point (MDP) simulations consisting of three points: sea-level static (SLS), top of climb (TOC), and beginning of cruise (CRZ). The subsonic variants' TOC and CRZ mission points are taken from a 737-800 mission profile generated by the SUAVE software [24]. As the SUAVE data used does not include a SLS point, the SLS thrust is assumed to be 91.46 kN based on an 15% de-rated takeoff for the CFM56-7B24 variant [25]. The SST variants use mission profile points from the NASA Supersonic Technology Concept Aeroplane (STCA) described in Berton et al. [26], [27]. The points chosen are outlined in Table 2.1. For the purposes of demonstrating MEM, it is assumed that changes to fuel burn rate will have negligible effects on thrust requirement to allow the propulsion sizing to be decoupled from airframe data.

An implementation of the Constrained Optimization by Linear Approximation (COBYLA) algorithm from the Python SciPy library is used in conjunction with NPSS to size all engines [28], [29]. Specifically, optimization is performed to minimize the thrust-specific power consumption (TSPC) [15] at CRZ. TSPC is defined as

$$TSPC = \frac{P_{tot}}{F_N} = \frac{u_0}{\eta_0} \tag{2.72}$$

Non-design variables cannot be rigidly constrained in the optimization scheme used. As such, soft constraints were placed on the problem by adding penalties to the objective function if the limits were exceeded. These penalties took the form

$$\ell_{max}(x_i) = w_i \max\left(\frac{x_i}{x_{i,max}} - 1, 0\right) \tag{2.73}$$

$$\ell_{min}(x_i) = w_i \max\left(\frac{x_{i,min}}{x_i} - 1, 0\right) \tag{2.74}$$

for a maximum or minimum limit, respectively. The variables x_i, $x_{i,max/min}$, and w_i rep-

resent the output variable of interests, the maximum/minimum allowable value for that variable, and the penalty scaling factor respectively. Given this, the objective function for minimization took the form:

$$f = TSPC_{CRZ} + \sum_{i=1}^{n} \ell_{max}(x_i) + \sum_{j=1}^{m} \ell_{min}(x_j) \tag{2.75}$$

for n maximum and m minimum constraints.

To decouple propulsion system sizing from airframe data, it is assumed for demonstration purposes that novel architectures (mixed flow, electric assist) will be retrofit onto an existing aircraft. The relative mass difference between a conventional and novel engine, Δm_{eng}, is then calculated and compared to a reference payload mass to determine the remaining payload fraction,

$$\delta m = 1 - \frac{\Delta m_{eng}}{m_{ref}} \tag{2.76}$$

For the subsonic engine variants, a 737-800 style aircraft with a per-engine payload capacity of 7500 kg is used [30]. The per-engine payload capacity for the SST engines is calculated from Berton et al. to be 248.0 kg [26]. Δm_{eng} for a given engine variant is composed of two primary components: difference in required fuel mass (Δm_{fuel}) and novel component mass (Δm_{novel}). Given the three prescribed mission points, it is assumed that the required fuel mass for the climb segment is approximated via trapezoidal integration of fuel flow rate over time:

$$m_{fuel,req} = \frac{\dot{m}_{f,TOC} + \dot{m}_{f,SLS}}{2}\left(t_{TOC} - t_{SLS}\right) + \frac{\dot{m}_{f,CRZ} + \dot{m}_{f,TOC}}{2}\left(t_{CRZ} - t_{TOC}\right) \tag{2.77}$$

This is calculated first for the optimized unmixed engine, giving a baseline fuel mass, $m_{fuel,0}$. Δm_{fuel} is then calculated for a given engine variation as

$$\Delta m_{fuel} = m_{fuel,req} - m_{fuel,0} \tag{2.78}$$

Unless otherwise stated, the fuel mass and remaining payload fraction are calculated based on the takeoff and climb segment of flight. For the hybrid electric variant, we also calculate

the difference in cruise fuel mass for comparison to literature. The trapezoidal integration assumption is not appropriate for more rigorous analyses. For these demonstrator examples it is sufficient, but for future work a more detailed fuel mass calculation should be used.

The novel component mass is dependent on specific engine architecture. We assume that changes to the mass of components common across variants will be negligible in comparison to added component mass such that we can forego dry mass estimation. Using the remaining payload fraction, the operational cost of novel engine implementations can be quantified. The following sections detail each of the selected engine architectures, their MEM models, and novel component masses (if applicable).

2.3.1 Subsonic unmixed engine

A diagram of the unmixed subsonic engine is shown in Figure 2.13. We assume that the root of the fan acts as a part of the low-power compressor (LPC). Note that the low power turbine is split between the gas generator and the power turbine, with the boundary point defined as station 4.7. This boundary is not a set physical location in the turbine, but instead represents the split in LP shaft power demanded by the core versus that demanded by the bypass stream. This provides a powerful way of separating streamwise energy flow.
The MEM expression for this engine is

$$\eta_0 = \eta_p \left[\kappa_{5.1-2}^{9-0} \left((1 - E_p)\eta_{gg} H_p^{gg} + \chi_{bld} B_p \epsilon_{bld} \right) + \kappa_{13.5-12}^{19-10} (1 - B_p)\epsilon_{bld} \right] \tag{2.79}$$

where

$$\epsilon_{bld} = \kappa_{13-12}^{13.1-12} \eta_{fan} \eta_{pt} E_p \eta_{gg} H_p^{gg} \tag{2.80}$$

We assume that the only power source for this architecture is fuel, such that $H_p^{gg} = 1$. Equation 2.79 has three primary terms: a primary core term, $(1 - E_p)\eta_{gg}$, a core bleed term, $\chi_{bld} B_p \epsilon_{bld}$, and a bypass term, $\kappa_{13.5-12}^{19-10}(1 - B_p)\epsilon_{bld}$. As a conventional engine, this system has no novel components to construct weight models for. The design variables and limits used in optimization are listed in Table 2.2.

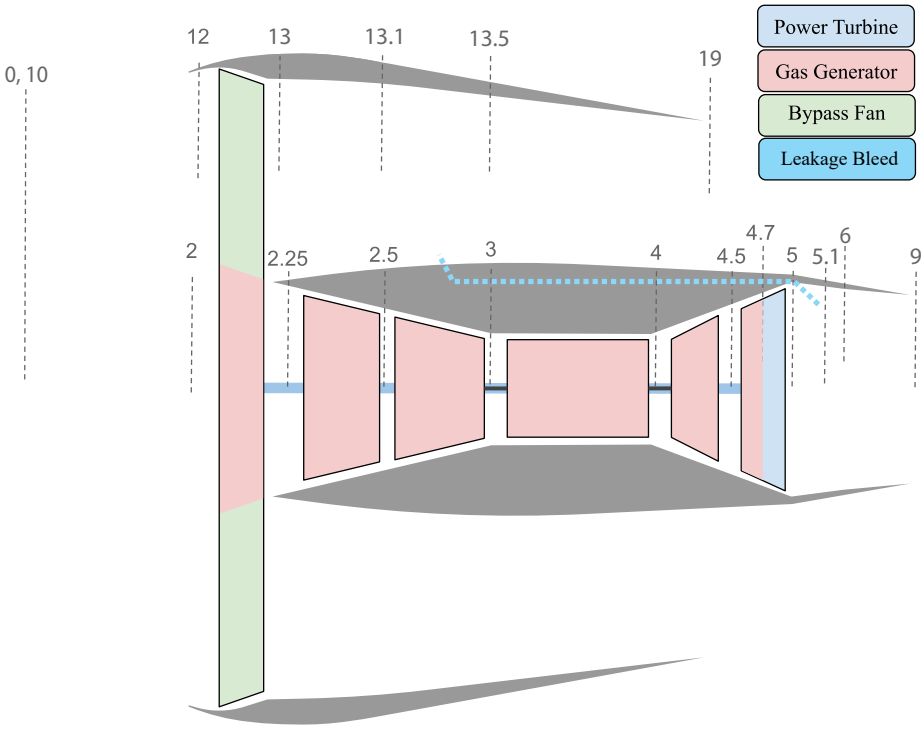

Figure 2.13: Subsonic unmixed engine diagram.

Table 2.2: Unmixed subsonic optimization variables and limits.

Optimization Variables				Limits		
Point(s)	Variable	Maximum	Minimum	Point(s)	Variable	Maximum
TOC	π_{fan}	2.0	1.4	TOC, SLS, CRZ	T_{t3}	900 K
TOC	π_{lpc}	–	1.1	TOC, SLS, CRZ	HPT T_{blade}	1222 K
TOC	π_{hpc}	–	8	TOC, SLS, CRZ	HPT T_{vane}	1278 K
TOC	$T_{t4.1}$	2000 K	1278 K			
TOC	d_{fan}	2.06 m	1.02 m			

2.3.2 SST unmixed engine

The unmixed SST engine is nearly identical to the subsonic engine shown in Figure 2.13. However, travelling at supersonic speeds leads to much higher levels of ram compression than is seen in subsonic engines. As such, a low pressure compressor is not needed for charging the core flow. From the perspective of the MEM gas generator grouping, the energy flow has not changed, meaning MEM for the SST unmixed engine is identical to that of the subsonic unmixed engine, given by Equations 2.79 and (2.80).

While the nominal engine for the NASA STCA includes a lobed flow mixer, we assume

Table 2.3: Unmixed SST optimization variables and limits.

Optimization Variables				Limits		
Point(s)	Variable	Maximum	Minimum	Point(s)	Variable	Maximum
TOC	π_{fan}	2.2	1.8	TOC, SLS, CRZ	T_{t3}	900 K
TOC	π_{hpc}	–	8	TOC, SLS, CRZ	HPT T_{blade}	1222 K
TOC	$T_{t4.1}$	2000 K	1278 K	TOC, SLS, CRZ	HPT T_{vane}	1278 K
TOC	d_{fan}	1.52 m	1.14 m			

that the payload mass cited in Berton et al. [26] would be approximately equal to that of a design for unmixed engines. Otherwise, there are no novel components to address in this engine. Due to flying in the supersonic regime, supersonic drag sources, such as wave drag, are incurred. For supersonic flight, thrust requirements are modified by an estimate of the change in wave drag due to changes in inlet geometry, parameterized by fan diameter [31], [32]. The particular details of this estimate can be found in Appendix C. The optimization variables and limits used to size this architecture are outlined in Table 2.3.

2.3.3 Subsonic mixed-flow engine

A diagram of the mixed flow subsonic engine is shown in Figure 2.14. This engine is identical to the unmixed equivalent, with the exception that the flows at stations 6 and 16 are combined using a lobed flow mixer into a single output at station 7. The addition of a well-designed flow mixer to an engine can improve thrust-specific fuel consumption [33] and thus also improve TSPC.

The MEM expression for this engine is

$$\eta_0 = \eta_p \kappa_{6,16-2,12}^{9-0,10} \left[\kappa_{5.1-2}^{6-2} \left((1 - E_p)\eta_{gg} H_p^{gg} + \chi_{bld} B_p \epsilon_{bld} \right) + \kappa_{13.5-12}^{16-12} (1 - B_p)\epsilon_{bld} \right] \tag{2.81}$$

where

$$\epsilon_{bld} = \kappa_{13-12}^{13.1-12} \eta_{fan} \eta_{pt} E_p \eta_{gg} H_p^{gg} \tag{2.82}$$

Note that the inner efficiency term in Equation 2.81 takes the same form as the unmixed variant in Equation 2.79. The primary difference comes in the static loss fractions. For the

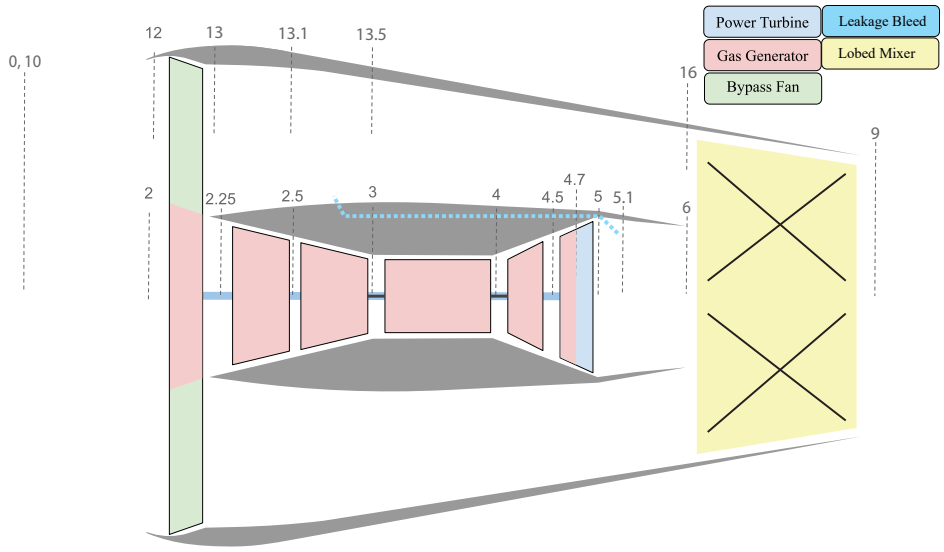

Figure 2.14: Subsonic mixed flow engine diagram.

mixed engine, there is now a leading κ equal to

$$\kappa_{6,16-2,12}^{9-0,10} = \frac{\eta_{noz}\chi_{mix}(\sigma_6 + \sigma_{16}) + \sigma_{overboard} - \eta_{in}^{-1}(\sigma_0 + \sigma_{10})}{\Delta\sigma_{6-0} + \Delta\sigma_{16-10}} \tag{2.83}$$

This is where the mixer effectiveness is introduced. The static loss fractions inside the inner efficiency expression then account for ducting just before the lobed mixer.

Flow mixer total mass is composed of the lobed mixer mass and the extra nacelle mass. The lobed mixer is assumed to be made of 0.1 in steel with surface area estimated using inner, mid, and outer radii (R_i, R_m, R_o); number of flow passages (N); and length (L) [34]:

$$S = 0.028L\big(3.93R_m + 1.25N(R_o - R_i)\big) \quad [\text{in}^2] \tag{2.84}$$

The units in variables in Equation 2.84 are assumed to be in inches except for N, which is dimensionless. We assume that the density of steel is approximately 7850 kg/m^3 [35]. Based on images and measurements from *Jane's Aero Engines* [25], a conservative mixer length was determined to be $L = 1.14$ m. The radii are estimated using the flow area at the LPT exit calculated by NPSS as well as estimation of a turbine exit hub-to-tip ratio of 0.67 using images from *Jane's*. The number of flow passages is taken to be 12. For the nacelle weight, we use the simple cylinder model outlined by Jackson [36], where the nacelle

Table 2.4: Mixed-flow subsonic optimization variables and limits.

Optimization Variables				Limits		
Point(s)	Variable	Maximum	Minimum	Point(s)	Variable	Maximum
TOC	π_{fan}	2.0	1.4	TOC, SLS, CRZ	T_{t3}	900 K
TOC	π_{lpc}	–	1.1	TOC, SLS, CRZ	HPT T_{blade}	1222 K
TOC	π_{hpc}	–	8	TOC, SLS, CRZ	HPT T_{vane}	1278 K
TOC	$T_{t4.1}$	2000 K	1278 K	TOC	d_{fan}	2.06 m
TOC	Extr. Ratio	1.1	0.9			

Table 2.5: Mixed-flow SST optimization variables and limits.

Optimization Variables				Limits		
Point(s)	Variable	Maximum	Minimum	Point(s)	Variable	Maximum
TOC	π_{fan}	2.2	1.8	TOC, SLS, CRZ	T_{t3}	900 K
TOC	π_{hpc}	–	8	TOC, SLS, CRZ	HPT T_{blade}	1222 K
TOC	$T_{t4.1}$	2000 K	1278 K	TOC, SLS, CRZ	HPT T_{vane}	1278 K
TOC	Extr. Ratio	1.1	0.9	TOC	d_{fan}	1.52 m

diameter is equal to $2R_o$ and the additional nacelle length is equal to that of the mixer. The optimization variables and limits used to characterize this mixed-flow architecture are listed in Table 2.4.

2.3.4 SST mixed flow engine

As in the unmixed case, the SST mixed flow engine is identical to the subsonic equivalent shown in Figure 2.14, except for the absence of the LPC. We also know that the path of energy flow, and thus the MEM expressions, for the engines are identical. As such, the MEM expression for a mixed flow SST engine is given by Equations 2.81 and 2.82.

For mixer mass estimation, the length, hub-to-tip ratio, steel density, and number of passages from the subsonic mixed-flow engine are used. This reduces the mixer mass to a function of power turbine exit area. The optimization variables and limits for sizing this engine are listed in Table 2.5.

2.3.5 Subsonic parallel hybrid engine

An engine diagram of the subsonic parallel hybrid electric engine is shown in Figure 2.15. We assume a gas turbine architecture identical to the unmixed subsonic variant. The primary

difference is the presence of a battery powered electric motor adding additional shaft power to the low-power shaft via a mechanical differential. Motor power is attributed to the bypass fan, with the low-power compressor still being part of, and thus having its power supplied by, the gas generator. Assuming the gas generator is powered by fuel and the electric motor is powered by batteries carried onboard, the MEM expression for this architecture is

$$\eta_0 = \eta_p \left[\kappa_{5.1-2}^{9-0} \left((1 - E_p)\eta_{gg} H_p^{gg} + \chi_{bld} B_p \epsilon_{bld} \right) + \kappa_{13.5-12}^{19-10} (1 - B_p)\epsilon_{bld} \right] \tag{2.85}$$

where

$$\epsilon_{bld} = \kappa_{13-12}^{13.1-12} \eta_{fan} \eta_{diff} \left[\eta_{pt} E_p \eta_{gg} H_p^{gg} + \eta_{mot} H_p^{bat} \right] \tag{2.86}$$

Note that the overall efficiency expression has the same form as the unmixed non-hybrid equivalent. The primary difference is in the bleed power fraction, which includes three new terms: η_{diff}, η_{mot}, and H_p^{bat}. The first is the efficiency of the mechanical differential used to sum the motor and LP shafts. The second is the electric-to-shaft power efficiency of the motor, and the final is the battery degree of power hybridization, $H_p^{bat} = P_{bat}/P_{tot}$. The contributions from the motor only appear in the bleed power fraction, reflecting the attribution of the motor power entirely to the bypass. This definition means the motor power only affects the bypass stream power fraction and the cross-stream leakage bleed, which we see reflected in the MEM expression.

The novel component mass of this architecture is composed of two primary components: electrical motor mass and battery mass. Motor mass is calculated using the methods outlined in Dowdle et al. [37]. The battery mass is determined by the assumed technology level of the batteries used, parameterized by specific energy (E^* [Wh/kg]) and specific power (P^* [W/kg]). For a given technology level, the battery mass is taken to be

$$m_{bat} = \max\left(\frac{E_{bat}}{E^*}, \frac{\max_i(P_i)}{P^*} \right) \tag{2.87}$$

for $i \in$ [SLS, TOC, CRZ]. Battery technology level is chosen based on ranges for lithium ion batteries from Šimić et al. [38]. The selected values represent modern battery technology and are $E^* = 200\,\text{Wh/kg}$ and $P^* = 1200\,\text{W/kg}$.

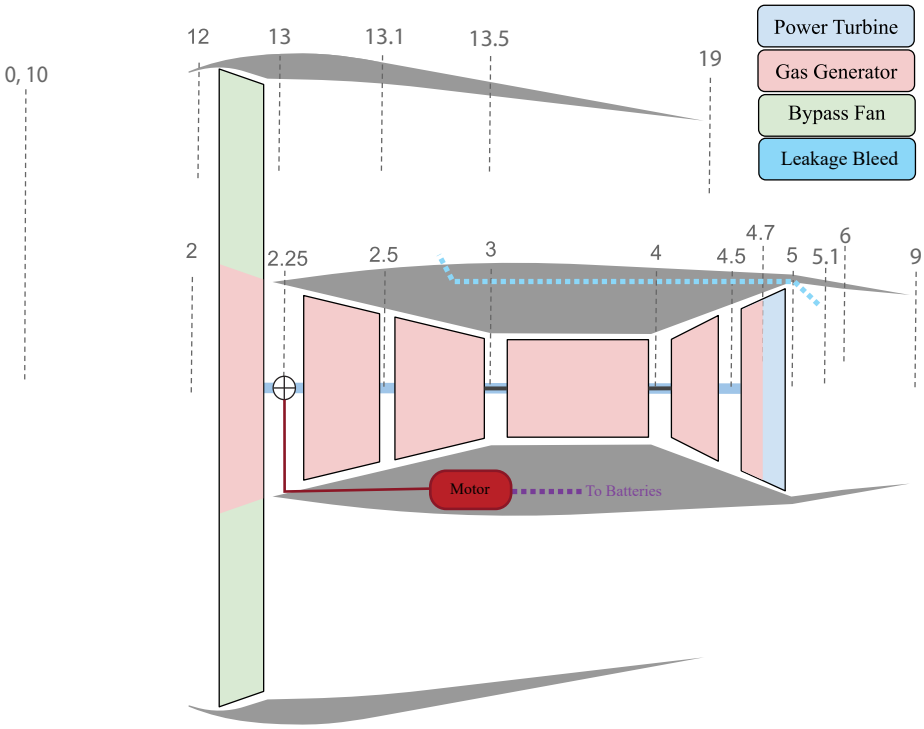

Figure 2.15: Subsonic parallel hybrid electric engine diagram.

To obtain the battery energy requirement, trapezoidal integration of the battery power over the three mission points is used. We assume that the engine has sufficient thrust at SLS and CRZ such that hybridization is not immediately needed. We then assume that the battery degree of power hybridization increases linearly to the value at TOC before linearly decreasing back to zero at CRZ. It should be noted that to ensure convergence of the NPSS solver, a minimum value of $H_p^{bat} = 0.001$ is used to approximate a zero-hybridization condition. In future work, it would be meaningful to look at the effect of raising the battery degree of power hybridization at SLS as well as attempting to use more mission points to define a more optimal $H_p^{bat}(t)$ profile.

Finally, we assume mass of wiring, power converters, and the mechanical differential will be small in comparison to these components. For future, more detailed analyses of hybrid electric systems, these masses should be accounted for. The optimization variables and limits for this engine are listed in Table 2.6.

Table 2.6: Parallel hybrid-electric subsonic optimization variables and limits.

Optimization Variables				Limits		
Point(s)	Variable	Maximum	Minimum	Point(s)	Variable	Maximum
TOC	π_{fan}	2.0	1.4	TOC, SLS, CRZ	T_{t3}	900 K
TOC	π_{lpc}	–	1.1	TOC, SLS, CRZ	HPT T_{blade}	1222 K
TOC	π_{hpc}	–	8	TOC, SLS, CRZ	HPT T_{vane}	1278 K
TOC	$T_{t4.1}$	2000 K	1278 K			
TOC	d_{fan}	2.06 m	1.02 m			

2.4 Performance metrics

To facilitate meaningful and rapid evaluation of propulsion system efficiency and behavior using MEM, several additional performance metrics are defined. These are relative power dissipation, $\delta\eta_i$, individual powertrain efficiency, η_0^i, the degree of thrust hybridization, H_F^i, and the stream power fraction ratios, ε_i^j and $\hat{\varepsilon}_i^j$. The definitions and use cases for these metrics are explained below.

2.4.1 Relative power dissipation

Relative power dissipation metrics provide a way to characterize the power dissipated in a given component (or collection of components) relative to the total system source power. This allows rapid identification of which components are responsible for the largest losses and which losses are the most sensitive to design/mission parameters.

The relative power dissipation of a component, i, with efficiency η_i is defined as

$$\delta\eta_i = (1-\eta_i)\epsilon_{input} \tag{2.88}$$

where ϵ_{input} is the input power fraction to that component. For example, the power turbine from the hybrid-electric engine in Figure 2.15 has a relative power dissipation of

$$\delta\eta_{pt} = (1-\eta_{pt})E_p\eta_{gg}H_p^{gg} \tag{2.89}$$

Relative power dissipation is defined identically for component effectiveness, χ_i, and static

loss fractions, κ. For component effectiveness, it is possible for the relative power dissipation to be negative. This indicates that a particular component is recovering some amount of power that would otherwise be dissipated. A common example of this are flow mixers, which act to increase thrust of the mixed streams [33], effectively recovering some flow power. It should be noted that relative power dissipation specifically refers to flow power. Exergy dissipation would be strictly positive.

For static loss fractions, relative power dissipation is the sum of relative dissipation incurred by the constituent static components. For example, in a system consisting of a lossy inlet and a nozzle,

$$\delta\kappa = (1-\kappa)\epsilon_{input} \tag{2.90}$$

$$\delta\kappa = \left(1 - \frac{\eta_{noz}\sigma_{noz} - \eta_{in}^{-1}\sigma_{in}}{\Delta\sigma_{noz-in}}\right)\epsilon_{input} \tag{2.91}$$

$$\delta\kappa = \delta\eta_{noz}\epsilon_{noz} + \delta\eta_{in}\epsilon_{in} \tag{2.92}$$

All relative power dissipation terms will sum to $1 - \eta_0$, representing the total source power minus the useful thrust power.

2.4.2 Powertrain efficiency and degree of thrust hybridization

Powertrain efficiencies are defined as the efficiency with which a particular power source is converted to thrust, allowing detailed examination of individual source power conversion pathways. If a MEM expression has been found for a system with n power sources the terms can be grouped to isolate the individual degrees of power hybridization. The resulting form is a sum of powertrain efficiencies weighted by degrees of power hybridization:

$$\eta_0 = \eta_0^0 H_p^0 + \eta_0^1 H_p^1 + ... + \eta_0^{n-1} H_p^{n-1} \tag{2.93}$$

This representation allows system efficiency to be viewed as an average of indivudal powertrain efficiencies, weighted by their respective degree of power hybridization. From this form, another metric can be extracted. Each powertrain efficiency represents conversion of

a particular source power to thrust. If we expand the overall efficiency into a sum of thrusts attributable to each power source, we get a sum of the form

$$\eta_0 = \frac{F_N^0 u_0}{P_{tot}} + \frac{F_N^1 u_0}{P_{tot}} + ... + \frac{F_N^{n-1} u_0}{P_{tot}} \tag{2.94}$$

Using the degrees of power hybridization, this can be rewritten as

$$\eta_0 = \frac{F_N^0 u_0}{P_0} H_p^0 + \frac{F_N^1 u_0}{P_1} H_p^1 + ... + \frac{F_N^{n-1} u_0}{P_{n-1}} H_p^{n-1} \tag{2.95}$$

where the $F_N^i u_0 / P_i$ terms in this series are the powertrain efficiencies. Dividing by η_0, the sum becomes ratios of thrusts:

$$1 = \frac{F_N^0}{F_N} + \frac{F_N^1}{F_N} + ... + \frac{F_N^{n-1}}{F_N} \tag{2.96}$$

The terms in Equation 2.96 represent the fraction of the total thrust attributable to a given power source, with the property that the sum of all such fractions will be one. We call these terms degrees of thrust hybridization, defined as

$$H_F^i = \frac{F_N^i}{\sum_{i=0}^{n-1} F_N^i} \tag{2.97}$$

Among other applications, these can be used to directly assess the contributions of a given powertrain to thrust or to constrain a particular power source's thrust production during sizing.

2.4.3 Stream power fraction ratios

Stream power fraction ratios measure the relative flow power contributions of two streams in a system. For two streams, 0 and 1, the stream power fraction ratio is defined as

$$\varepsilon_0^1 = \frac{\epsilon_1^{st}}{\epsilon_0^{st}} \tag{2.98}$$

When the value of Equation 2.98 is less than one, stream 0 is producing a larger flow power rise. When it is greater than one, stream 1 is producing the greater flow power rise. This quantity is especially useful in analyzing core/bypass two-stream systems, such as turbofans, to understand whether the high specific flow power core or low specific flow power bypass is dominating the overall flow power production. A related metric is the specific stream power fraction ratio, which is defined as the ratio of specific flow power rise in each stream:

$$\hat{\varepsilon}_0^1 = \frac{\hat{\epsilon}_1^{st}}{\hat{\epsilon}_0^{st}} \tag{2.99}$$

Here, $\hat{\epsilon}$ refers to the mass specific stream power fraction, $\hat{\epsilon} = \Delta\hat{\sigma}/(P_{tot}/\dot{m})$. This term represents the ratio of flow power added per unit mass to each stream, which is a more useful form when considering the thermodyamic representations of the streams.

2.5 Methodology summary

In this chapter, we define new metrics for tracking power in propulsive flows (σ, H_p^i) and use those metrics to define the efficiencies, effectiveness, and related quantities for general components in a propulsion system. Using the component definitions, expressions for overall efficiency could be constructed which used consistent metrics across any architecture to an arbitrarily fine level of detail, constituting the Modular Efficiency Model. We then presented the five engine architectures used to demonstrate the use of MEM, consisting of both subsonic and SST unmixed and mixed-flow engines as well as a subsonic unmixed hybrid-electric engine. Finally, we presented three more complex performance metrics that will be key in understanding the behavior of the examined engines. Based on these methods, we will now evaluate the performance of each engine variant. Specifically, these architectures will be compared based on MEM metrics, required takeoff/climb fuel mass, and remaining payload after a retrofit.

Chapter 3

Results

3.1 Evaluation of unmixed and mixed-flow turbofan performance

Key efficiencies and performance parameters for each engine are summarized in Table 3.1. In both SST and subsonic engines, the mixed-flow engine performed better on overall efficiency and TSPC bases. In particular, the mixed-flow SST engine had a 2.2% increase in overall efficiency while the subsonic mixed-flow engine only exhibited a 0.8% increase. We now look at each class of engine and use MEM to understand where they derive particular efficiency increases. After this, a comparison of the two mixed-flow engines is done to determine some conditions for good lobed-mixer applications.

3.1.1 Subsonic engines

The mixed flow subsonic engine's overall efficiency increase was primarily driven by propulsive efficiency, which increased over the unmixed equivalent at TOC by 2.1%. In comparison, the inner efficiency dropped by 0.2%. This small decrease is most likely rooted in the decreases in OPR and T_{t41}/T_{t2} of the mixed-flow engine. However, for such significant drops in both quantities we would normally expect a larger decrease in inner efficiency. The relative power dissipation, as defined in Section 2.4.1, due to engine components is summarized in Figure 3.1. We see that the gas generator power dissipation increases at all mission points, with

Table 3.1: Design/performance parameters for unmixed and mixed engines at TOC.

	Subsonic		SST	
	Unmixed	Mixed	Unmixed	Mixed
Fan Pressure Ratio, π_{fan}	1.55	1.44	2.17	1.80
Overall Pressure Ratio, OPR	56.7	43.8	27.5	28.9
TET Ratio, T_{t41}/T_{t2}	8.17	7.16	6.22	6.63
Fan Diameter, d_{fan} [m]	2.050	2.054	1.404	1.257
Thrust Specific Power Consumption, $TSPC$ [kW/N]	0.663	0.648	1.097	1.035
Overall Efficiency, η_0	0.341	0.349	0.377	0.399
Propulsive Efficiency, η_p	0.767	0.788	0.751	0.741
Inner Efficiency, η_{inner}	0.445	0.443	0.502	0.539
Stream Power Fraction Ratio, ε_{core}^{byp}	5.52	2.24	3.27	0.83
Specific Stream Power Fraction Ratio, $\hat{\varepsilon}_{core}^{byp}$	0.362	0.165	0.531	0.141
Bypass Ratio, α	15.24	13.54	6.15	5.90
Turbine Extraction Fraction, E_p	0.88	0.76	0.80	0.51
Mixer Effectiveness, χ_{mix}	–	0.995	–	1.012
Remaining Payload Fraction, δm	–	0.987	–	1.083
Mixer Mass, m_{mix} [kg]	–	112.0	–	55.0
Required Fuel Mass Change, Δm_{fuel} [kg]	–	-13.3	–	-75.5

the difference between the unmixed and mixed values differing by more than 0.2%. Looking specifically at TOC, the increase in gas generator power dissipation is approximately 1%, about five times higher than the decrease in inner efficiency would suggest.

As such, the increased gas generator losses must be offset by gains in other components. The first such component is the power turbine, whose relative dissipation drops by 0.7% in the mixed case. The power turbine (flow power) efficiencies are approximately equal, implying that less flow power is being converted to shaft power by the device even though the core size grows (decrease in α). The decrease in power turbine dissipation indicates a lower turbine extraction fraction, E_p, which we can confirm is the case in Table 3.1. The fan power dissipation also drops by 0.55% when sizing the mixed engine. The increase in fan diameter (and thus mass flow) and a relatively large drop in fan relative dissipation results in the drop in fan pressure ratio from 1.55 to 1.44. The decreases in fan and power turbine dissipation combine to offset the increased gas generator losses. However, the an increase in core size and a decrease in E_p would indicate an increase in jet velocity and a resulting decrease in propulsive efficiency. However, the flow mixer has an effectiveness less than unity. This implies that the flow mixer decreases the mass-averaged velocity of the

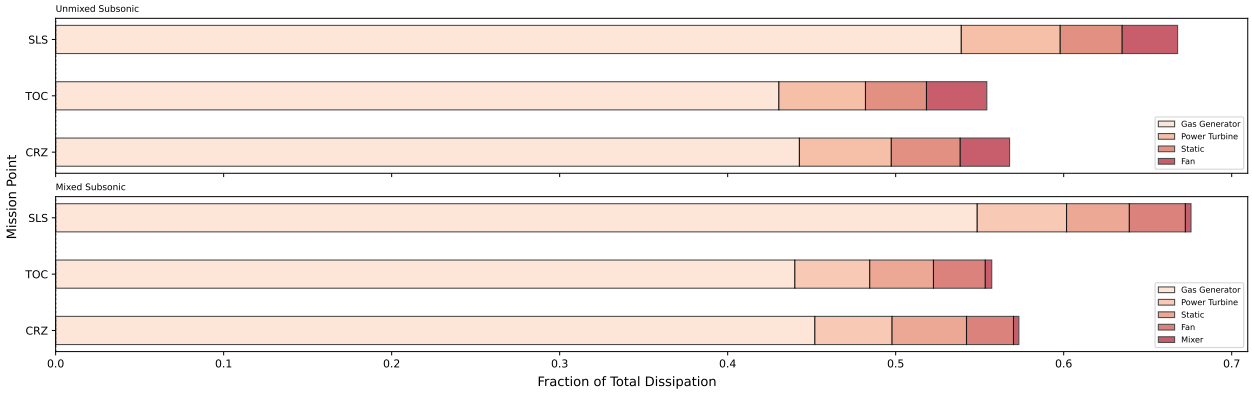

Figure 3.1: Relative power dissipation in unmixed and mixed-flow subsonic components.

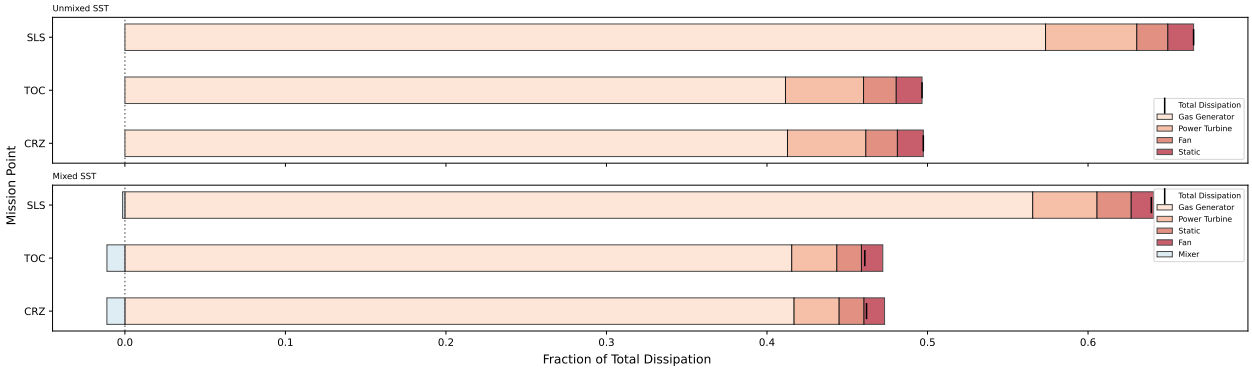

Figure 3.2: Relative power dissipation in unmixed and mixed-flow SST components.

streams. Combining this velocity decrease with the marginally higher mass flow leads to the slight propulsive efficiency increase seen in the results.

3.1.2 SST engines

The mixed flow SST engine's overall efficiency increase is primarily derived from improvements to inner efficiency (+3.7%) at the cost of decreased propulsive efficiency (−1.0%). This is the opposite of the case seen in the subsonic engines, where propulsive efficiency increased while inner efficiency decreased. The propulsive efficiency decrease comes from mixer effectiveness being greater than unity. For $\chi_{mix} > 1$, the jet velocity increases relative to the mass-averaged velocity of the individual streams. The primary benefit of the SST mixed flow engine is in inner efficiency. The component relative dissipation is shown in Figure 3.2. Three components provide the majority of the decrease in power dissipation: the power turbine, fan and mixer.

The decrease in power turbine dissipation is primarily a result of the decrease in turbine extraction from 80% to 51% while power turbine (flow power) efficiency remains approximately constant. As we leave more flow power in the core stream, less power is dissipated in the flow-to-shaft conversion process. The mixed engine's power turbine dissipates just over half of the power dissipated by the unmixed equivalent. For the fan, π_{fan} decreases from 2.17 to 1.8 while the flow power efficiency remains approximately constant. Combined with the reduced turbine extraction and smaller fan diameter, less power must be delivered to the fan. The net effect is a fan dissipating only 65% of the power dissipated by the unmixed engine's fan.

However, the changes described above greatly decrease the bypass thrust while the core thrust increase is small due to low core mass flow. It is the flow mixer that allows the system to meet the thrust requirement given the otherwise reduced thrust. The mixer increases the flow power of the streams, such that some power is "recovered" in the mixing process. Remember that there is a component of the total availability, exergy, that is normally inaccessible to air-breathing propulsion systems: the thermal component. We cannot bring a propulsive jet to ambient temperature usefully and, as such, that portion of useful work is unavailable. The mixing process here converts some of that unavailable thermal power to flow power through mixing of flows with a large temperature difference, resulting in an increase in flow power, but still a decrease in exergy. The benefits are maximized by the low fan pressure ratio and low extraction ensuring the bypass and core are as cool and as hot as possible, respectively. In relative dissipation terms, an effective mixer manifests as a negative dissipation, colored in shades of blue and reducing the total relative dissipation attributable to the engine components.

As a final note on the SST mixed flow engine we look at the thrust requirement. Until now we have assumed thrust remains constant. However, the SST models include a thrust adjustment due to wave drag. This encourages lower fan diameters by decreasing thrust requirement. For the mixed engine's 10.5% decrease in fan diameter relative to the unmixed one, the thrust requirement decreases by 2.4% at TOC (equal to $\sim 604\,\mathrm{N}$). Even with the decreased thrust requirement, the reduction in fan diameter decreases the mass flow by a large enough margin that the averaged jet velocity still increases. This introduces a trade

between improved propulsive efficiency (lower thrust and χ_{mix}) and inner efficiency (access to thermal availability via high χ_{mix}). For the SST case, the high χ_{mix} case resulted in greater $TSPC$ improvements. The effect of fan diameter on drag is not currently captured for the subsonic cases. In future work, this effect should be captured as it may effect whether the subsonic mixed flow engine converges to $\chi_{mix} < 1$ versus $\chi_{mix} > 1$.

3.1.3 Lobed mixer applicability comparison

The two cases of mixed-flow engines looked at in this work demonstrate two different use cases for lobed mixers. The subsonic engines demonstrated flow mixer capability to decrease mass-averaged velocity of a flow, allowing for higher propulsive efficiency. However, the benefits of this use case are limited due to decreased inner efficiency, need for higher mass flow to compensate, and decreased payload capacity resulting from the mixer mass. The SST case demonstrated the capability of mixers to access some of the otherwise unavailable thermal component of exergy to increase net flow power, and thus improve inner efficiency by recovering power. This came at the cost of a slight decrease in propulsive efficiency as the jet velocity was increased. However, the net effect was an increase in overall efficiency 2.75 times greater for the SST engines. Combined with the fact that the subsonic engines have a much higher fan diameter, resulting in a much larger (and thus heavier) lobed mixer, the SST engine is much more justified in using a flow mixer. In particular, the decrease in climb fuel mass due to efficiency improvements is unable to exceed the mixer mass in the subsonic case, resulting in a payload fraction less than unity. In the SST case, the fuel burn benefit is significantly greater than the mixer mass, resulting in a payload fraction of 1.083 implying more passengers could be carried if the airframe had the capacity to do so. Based on the MEM analysis presented above, we conclude that lobed flow mixers are most applicable in cases of low fan diameter such that engines will have higher fan pressure ratios to minimize mixer mass. For both subsonic and SST engines, including cruise segment fuel mass reductions would improve the payload fraction. For the purposes of this demonstration, the climb segment analysis was the simplest meaningful case. In more detailed future studies of mixed flow engines, the fuel mass estimate should be refined and the entire mission fuel burn should be evaluated.

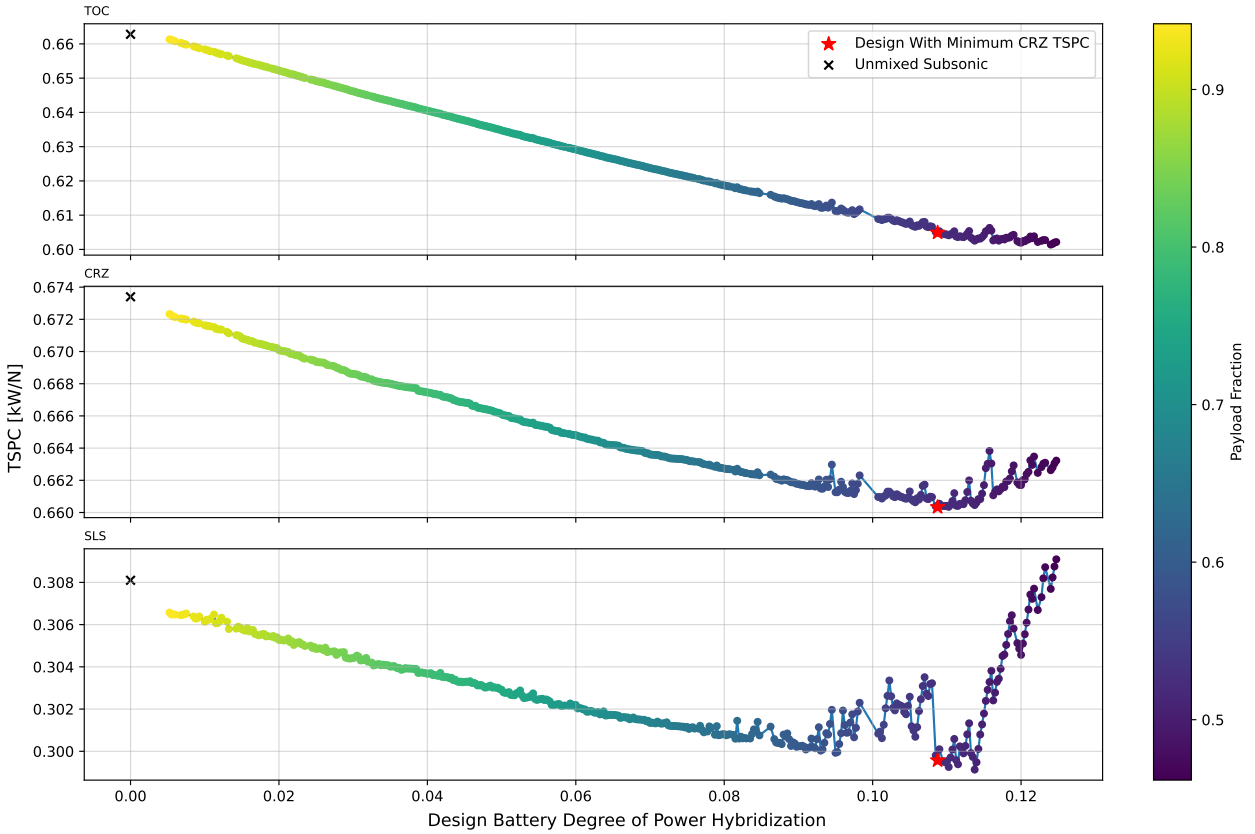

Figure 3.3: $TSPC$ improvement as a function of H_p^{bat} at TOC.

3.2 Effect of electrical hybridization

The hybrid-electric subsonic engine was evaluated at values of TOC battery degree of power hybridization between 0.5% and 12.5% with spacing of 0.025% without a payload fraction limit. The engine was assumed to operate without battery power at the SLS and CRZ points. The resulting $TSPC$ and change and required fuel mass for climb, cruise, and the whole mission are shown in Figures 3.3 and 3.4 respectively. The cruise segment fuel burn was estimated by assuming approximately constant fuel burn rate during the entirety of cruise.

There is considerable noise present in the SLS point data. This is due to the burner inlet temperature hitting the limiting value, discussed further in Section 3.2.2. There are also a number of gaps in the data at high values of H_p^{bat}. This is due to unconverged results from NPSS being rejected from the data set. Finally, if the data is extrapolated to $H_p^{bat} = 0$, it

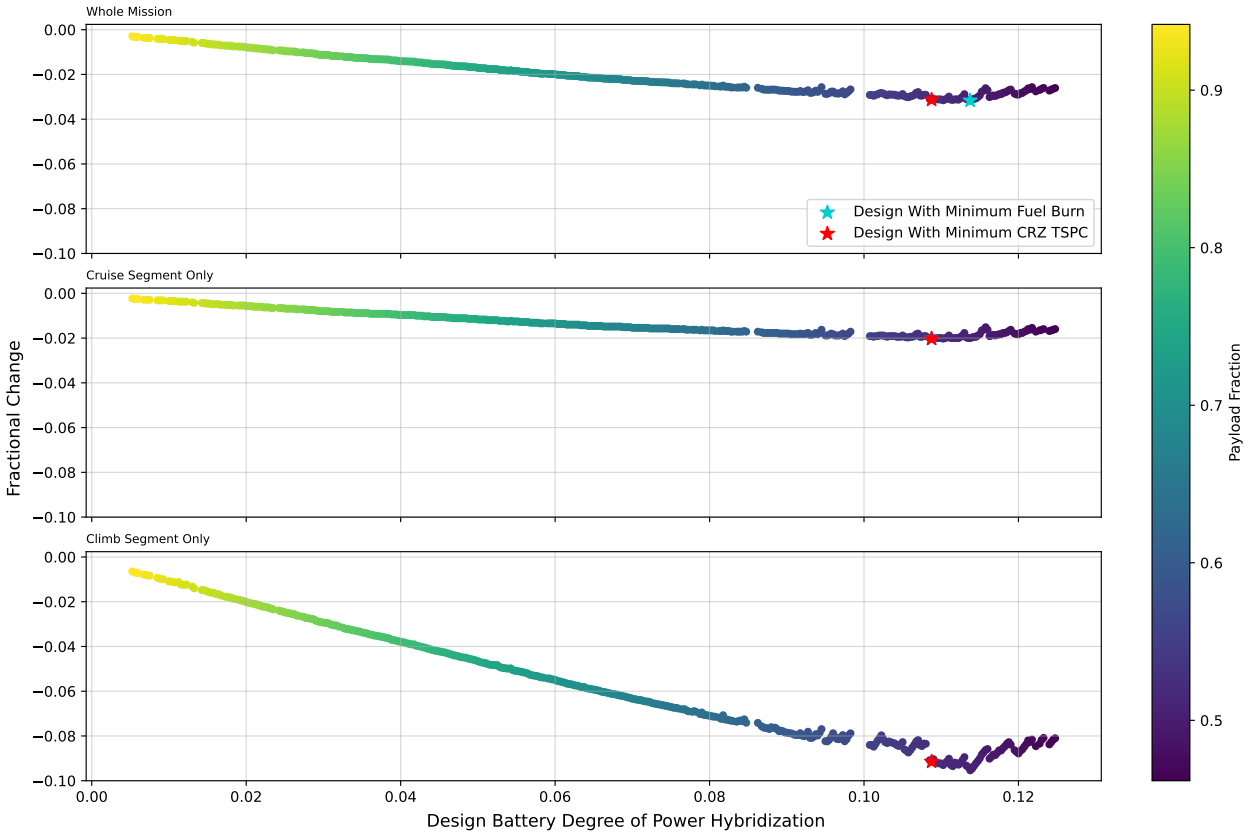

Figure 3.4: Fractional reduction in required fuel mass as a function of H_p^{bat} for climb, cruise, and the whole mission.

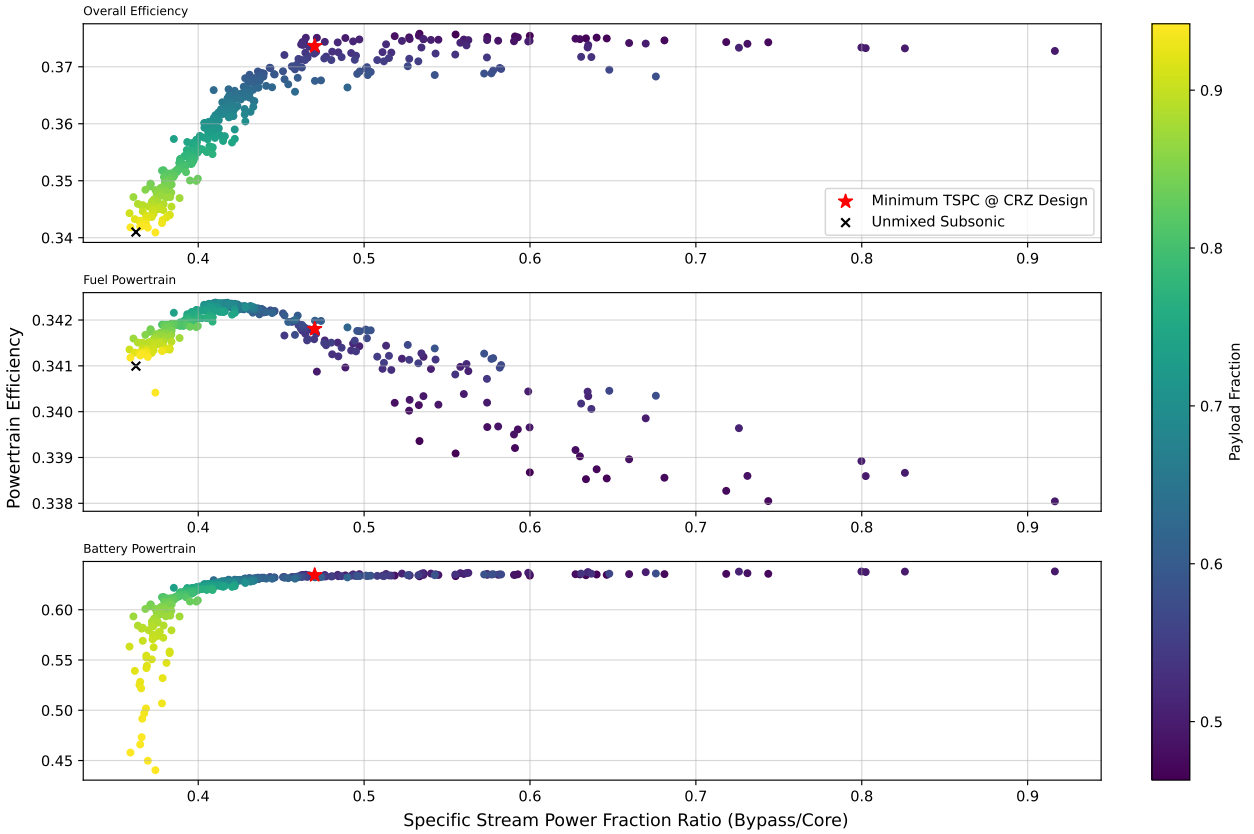

Figure 3.5: Individual powertrain efficiencies at TOC as a function of specific stream power fraction ratio.

closely approximates, but does not match, the unmixed engine results. This most likely due to the need to approximate the zero-hybridization conditions at SLS and CRZ as $H_p^{bat} = 0.1\%$ instead of truly ramping the hybridization to zero. In terms of fuel burn reduction, we see a best-case whole-mission fuel burn reduction of 3.2% at $H_p^{bat} = 11.375\%$, which is in the same range as the existing hybrid-electric studies presented in Chapter 1. However, this comes at the cost of an approximately 50% payload fraction. It is not economically feasible to halve the payload capacity of a commercial jet. As such, we recommend a more detailed study that includes airframe optimization be performed to confirm the magnitude of economically viable benefits. The remainder of this section explains the trends in $TSPC$ and fuel mass as well as techniques for a more detailed sizing from the lens of a MEM analysis.

First, looking at the data at TOC, we do not see a clear minimum. However, it is anticipated that if convergence at higher design H_p^{bat} values was achieved, we would see the curve reach a minimum before sharply rising. To understand this, the individual powertrain

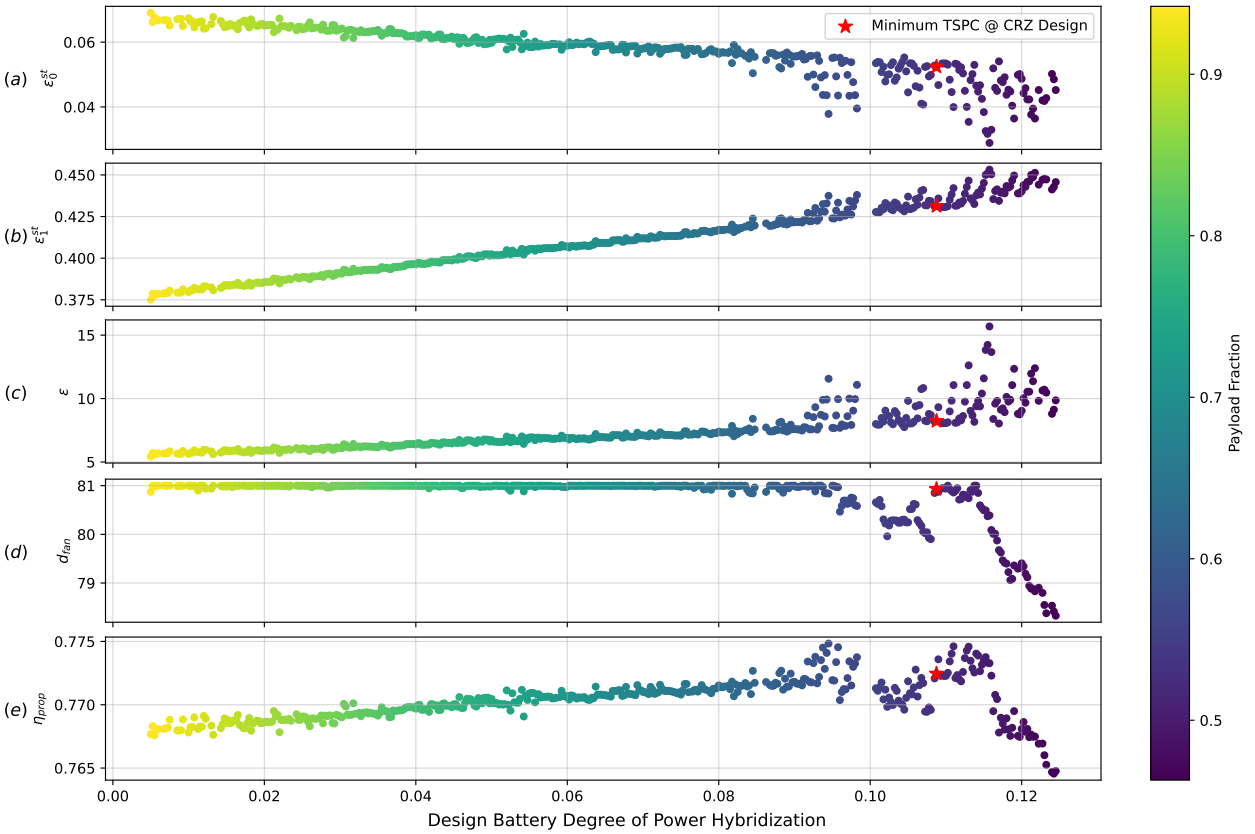

Figure 3.6: TOC core (a) and bypass (b) stream power fractions, stream power fraction ratio (c), fan diameter (d), and propulsive efficiency (e) as a function of design H_p^{bat}.

efficiencies are shown at TOC in Figure 3.5. Note that the point colors still correspond to the payload fraction, showing that increasing design H_p^{bat} correlates strongly with decreasing payload fraction. We see the battery powertrain efficiency rising sharply at low design H_p^{bat} before quickly approaching a maximum value. This is due to the electrical motor efficiency increasing to a maximum value as more shaft power is generated. This is in contrast to the fuel powertrain efficiency, which has a clear maximum at a stream power fraction around 0.41 (corresponding to design $H_p^{bat} \approx 9\%$) before sharply decreasing. Due to the much higher efficiency of the battery powertrain, as design H_p^{bat} increases, the weighted sum composing overall efficiency,

$$\eta_0 = \eta_0^{fuel} H_p^{fuel} + \eta_0^{bat} H_p^{bat}$$

weights battery powertrain efficiency with increasing strength. As such, even if fuel powertrain efficiency has a maximum at a lower H_p^{bat}, the maximum will lie at higher H_p^{bat}.

To understand why the fuel powertrain has a maximum efficiency as H_p^{bat} is increased at both TOC and CRZ, we turn to a number of metric shown in Figure 3.6 at TOC. We first see that the stream power fractions of the core (Figure 3.6a) and bypass (Figure 3.6b) monotonically decrease and increase respectively. This is due to the decreased load on the core, which is then given to the bypass fan via electrical power. This shrinks the gas generator size, increasing bypass ratio. The decrease in core size is reflected by the specific stream power fraction ratio (Figure 3.6c), which increases versus H_p^{bat} while fan diameter (Figure 3.6d) remains constant. The corrected speed of the fan is assumed to be at 100% at TOC. At high values of H_p^{bat}, increasing amounts of the fan work are provided by the electrical systems. As such, when the hybridization is turned off at CRZ, the corrected speed will decrease proportionally to the degree of battery power hybridization. The minimization of CRZ $TSPC$ ensures the fan pressure ratio is at it's lowest possible value for the highest possible fan diameter. As such, for a near constant fan pressure ratio, a decrease in corrected speed implies a decrease in mass flow. Eventually, this decrease in mass flow, combined with the decreasing core size, will result in the engine being unable to meet CRZ thrust requirements while keeping the fan diameter and pressure ratio constant. The only way to keep raising TOC hybridization, and thus $\hat{\varepsilon}_{core}^{byp}$, is to lower the fan diameter and increase core size. This decreases the propulsive efficiency (Figure 3.6e) via higher jet velocities, leading to the overall decrease in fuel powertrain efficiency seen at TOC and CRZ.

3.2.1 Detailed hybrid engine sizing using MEM

While this analysis has been done for a simple three-point model of a mission, it would be desired in a more detailed analysis to determine engine performance across a more granular climb profile in order to improve weight and fuel burn estimates. In particular, the task of determining the optimal H_p^{bat} profile across the climb is challenging. Using the current methods and solvers, multi-design point analysis would have to be performed at all points. This is computationally infeasible in terms of time and possibility of convergence. Instead, if the pinch points of the mission are identified (as done in this analysis) and the engine is sized initially using those points. It could then be possible to assess the degree of hybridization required at each mission point. In particular, if the gas turbine components are run in an

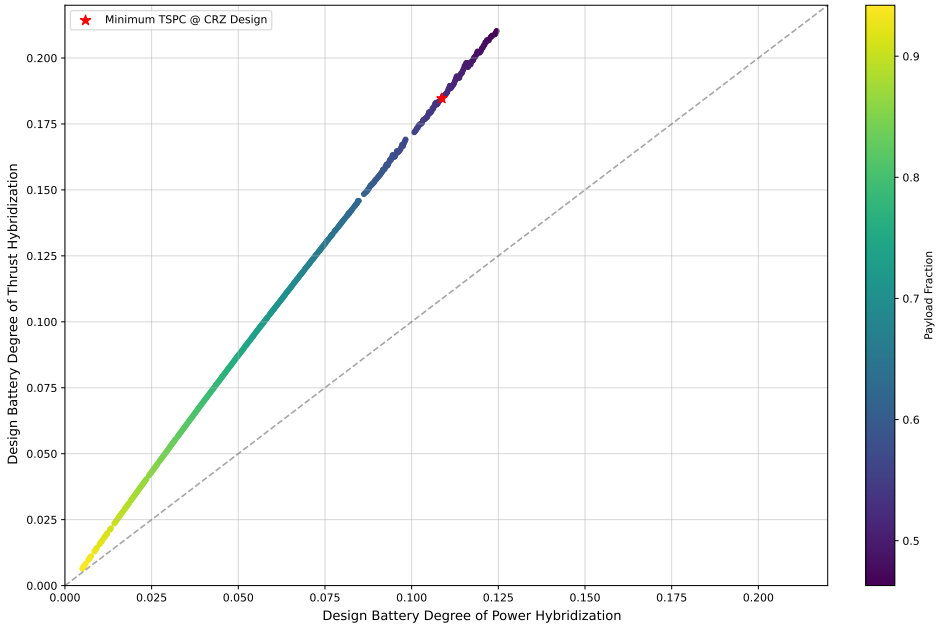

Figure 3.7: Degree of thrust hybridization increases faster than degree of power hybridization.

off-design sweep across the mission profile at maximum thrust conditions, we can obtain the maximum fuel-attributable thrust. With this, we can use the degree of thrust hybridization, H_F and individual powertrain efficiencies, to obtain the required degree of power hybridization given $F_{N,max}/F_{N,req}$ at a given point. This is an important step to take in order to account for differences in powertrain efficiencies. Namely, battery powertrains will almost always be more efficient than combustion powertrains. As such, every unit of power added by a battery system will generate more thrust than an identical unit of fuel power. This is seen in the current results, as shown in Figure 3.7. Using this method, H_p^{bat} profile optimization for minimum $TSPC$, fuel burn, or other metrics becomes computationally reasonable.

3.2.2 Artifacts and noise in hybrid-electric data

The MEM and true overall efficiencies of the hybrid-electric engine are plotted together as a function of H_p^{bat} at TOC in Figure 3.8. MEM demonstrates extremely good agreement with true overall efficiency for all cases. The sharp drop at the left end of the plot is representative of the first case at the lowest H_p being optimized using initial conditions far from the solution values. All steps after the first are performed using the previous solution as initial conditions.

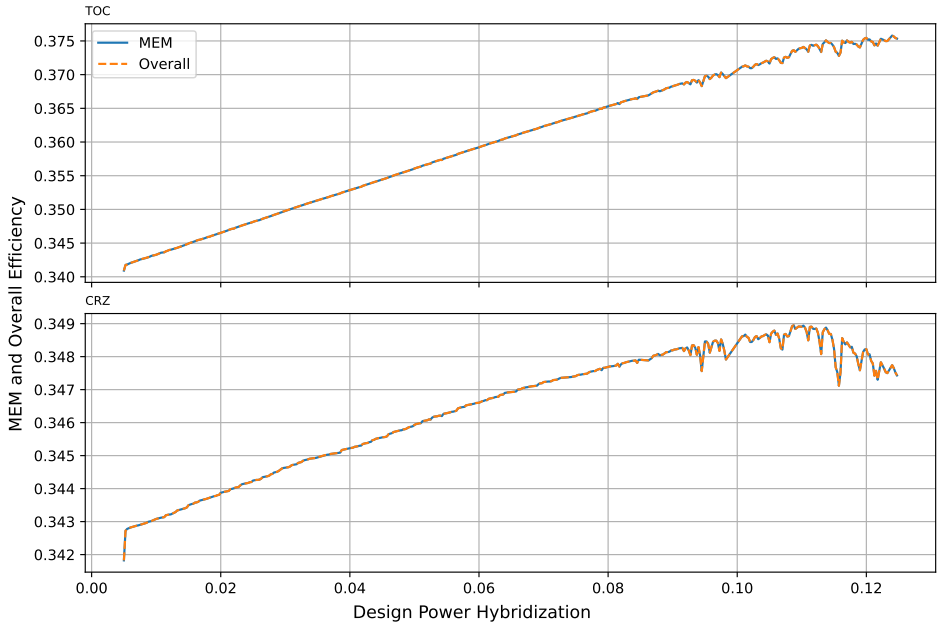

Figure 3.8: MEM and overall efficiency for a range of TOC H_p values in hybrid-electric engines.

As a result, the solution at the first H_p^{bat} is not able to fully settle to the true solution. As this is not a physical solution, the lowest H_p value is disregarded in analysis.

Finally, there is a significant amount of noise in the overall efficiency at TOC H_p^{bat} values greater than about 9%. This noise becomes significantly worse for the off-design efficiencies at CRZ. This is most likely due to the objective function definition for the COBYLA optimization. In particular, when one of the soft limits was reached, the resulting penalties caused noise in the objective function that translated to the final result. The constraint on burner inlet temperature (T_{t3}) at the sea level-static condition in particular is the only soft limit being reached during optimization. The TSPC at SLS initially follows a well-defined negative correlation with T_{t3} until reaching the limit of $900\,K$ where it becomes noisy, as shown in Figure 3.9.

Altering the weighting factor for the limit may reduce the magnitude of the noise, but could also effect whether the limit is maintained. For the purposes of this work, low noise data is not required as long as the trends in the data are clear. In this case, there is a clear near-linear rise in overall efficiency at CRZ until a maximum is reached. After this point, the efficiency begins to fall. As such, noise reduction was not pursued, but could be a goal

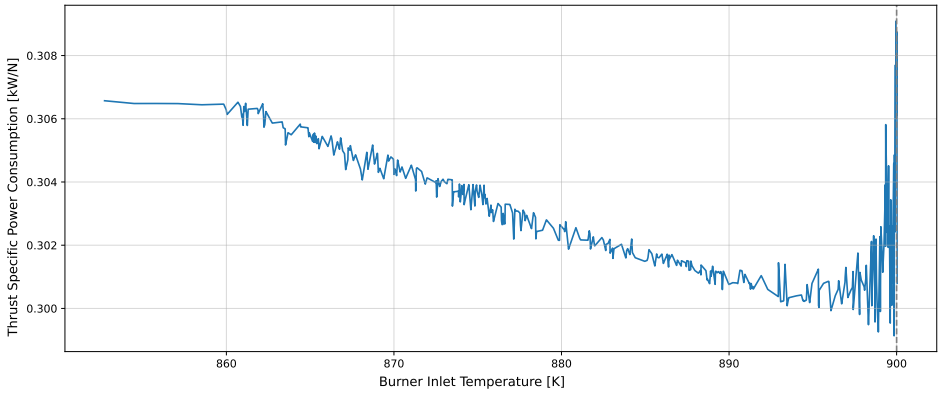

Figure 3.9: Noisy behavior of TSPC when T_{t3} approaches the limiting value.

of future work.

Chapter 4

Discussion & Conclusions

In this thesis, we present the Modular Efficiency Modeling, or MEM, framework for analysis, sizing and comparison of novel air-breathing propulsive architectures. To do this, a measure of available power in a propulsive stream, called expanded flow power, was defined and tracked on a component level throughout a given engine. This allows for component-level representations of energy conversion pathways in an engine, ensuring models of different novel systems, when represented by an assembly of components, could be compared on a 1-to-1 basis. While these models can become complex, two primary ways of collapsing the expressions emerged, each providing information about system performance.

The first simplification is the streamwise representation, where overall efficiency is written as a sum of stream power fractions:

$$\eta_0 = \eta_p \left[\epsilon_0^{st} + \epsilon_1^{st} + ... \right] \tag{4.1}$$

The form shown in Equation (4.1), alongside the stream power fraction ratios (ε, $\hat{\varepsilon}$), provides information on how effectively power is being generated in a given stream as well as how flow power is being distributed between different streams. The second simplification is the powertrain representation, where overall efficiency is written as an average of individual powertrain efficiencies weighted by degrees of power hybridization:

$$\eta_0 = \eta_0^0 H_p^0 + \eta_0^1 H_p^1 + ... \tag{4.2}$$

The form shown in Equation (4.2) provides insight about the efficiency and contributions of individual energy conversion pathways in systems with multiple input power sources. In addition, this form allows for the definition of the degree of thrust hybridization, useful in detailed sizing of hybrid systems.

Finally, the MEM framework was defined such that the relative power dissipation in individual components could be extracted, similar to existing exergy-based models [15]. These capabilities were demonstrated using two primary examples. First was a comparison of subsonic and supersonic aircraft propulsion systems with unmixed versus mixed propulsive streams. In particular, the low-level form was used alongside the relative power dissipation to understand the source of efficiency gains experienced in each Mach domain. We found that engines with smaller fan diameters, higher fan pressure ratios, and larger drag improvements from diameter reduction, like SST engines, experienced the greatest benefits from inclusion of lobed mixers. In particular, MEM allowed an understanding of how the 2.2% increase in overall efficiency and 1.08× payload increase were obtained.

The second example examined the application of hybrid-electric systems to a subsonic engine. We utilized MEM to explain the behavior of such systems at high degrees of battery power hybridization, where the maximum overall efficiency was reached. Specifically, we examined how the weighted-average effect in the powertrain representation leads to an efficiency maximum and looked at the low-level and streamwise representation to explain the maximum fuel powertrain efficiency. We found that it was possible to achieve a 3.2% reduction in whole-mission fuel-burn by retrofitting a 737-like aircraft with a hybrid propulsion system at the cost of a 50% payload fraction. This result is promising, but the low payload fraction indicates that a study where the entire aircraft is sized around the hybrid propulsion system instead of retrofit should be performed.

4.1 Future work

While MEM in it's current form is capable of representing fully generalized novel engines, a number of areas still need to be explored utilizing it in future work, presented below:

1. **Improvement to current assumptions.** The current work has two primary defi-

ciencies in the cycle decks used. First, the effect of increases to turbine active cooling flow are not modeled. Lee et al. [22] implemented a model for this effect based on work by Horlock and Torbidoni [39] as well as Hartsel [40] that was implemented externally to NPSS. This model will be implemented directly into NPSS for future work. In addition, the current work assumes no losses in propulsive nozzles. In reality, the nozzle exit velocity is scaled by some factors that will be represented in future work.

2. **Automation of MEM expression assembly.** Given that a systematic method of assembling MEM expressions is presented in this work, it should be possible to automatically generate these expressions in relevant analysis software, such as NPSS. This would greatly improve the usability of MEM and lower the barrier of entry to utilizing it. This would also eliminate potential human-error in modeling highly complex architectures.

3. **Full aircraft sizing implementation.** The work presented here assumed a retrofit of an existing aircraft with constant mission thrust to decouple from airframe data. It would be pertinent to perform a more generalized analysis of hybrid-electric systems in particular, where changes to aircraft performance were also captured, allowing for a comparison of systems with equal payload-range capabilities. In the short term, a sensitivity analysis of the current results to thrust requirement should be evaluated.

4. **Effect of improved battery technology.** The current hybrid-electric results examine only one case of battery specific power and energy. However, it is likely that on the timescale where hybrid-electric systems are implemented, battery technology could improve. As such, it is important to examine whether similar improvements can be made at higher payload fractions with future technology.

5. **Application to more systems.** While we investigate unmixed, mixed, and hybrid-electric engines in this work, more architectures should be examined using MEM. Two possible architectures are presented in Appendix A. This would expand the examples of MEM analysis, and allow for a deeper understanding of how these systems differ.

Appendix A

Additional Modeling Examples

During the study, two other novel architectures were discussed, but did not make it to the analysis phase. For the purposes of future analyses, their MEM expressions are provided here.

A.1 Turboelectric distributed propulsion

A diagram of a distributed turboelectric architecture is shown in Figure A.1. The specific configuration chosen is one where some number of gas generator/power turbine constructs, a each work to generate electrical power using generators. Each one is assumed to be powered by some fraction of the total source power such that each gas generator is described by a degree of power hybridization. This electrical power is merged into a central energy distribution and storage system, and is then distributed back to a number of electric motors coupled to fans (b) which are the primary propulsors. The energy storage system is assumed to dissipate some power as heat with efficiency $\eta_{storage}$. The MEM expression for this architecture is:

$$\eta_0 = \eta_p \left[\sum_{i=1}^{a} \left[\eta_{gg} H_p^{gg} (1 - E_p) \right]_i + \eta_{storage} \epsilon_{tot}^{elec} \sum_{j=1}^{b} w_j \left[\eta_{fan} \eta_{mot} \right]_j \right] \tag{A.1}$$

where w_j is a weighting factor describing the fraction of electrical power being delivered to propulsor j. These weighting terms are defined such that $\sum_{j=1}^{b} w_j = 1$. The ϵ_{tot}^{elec} term is

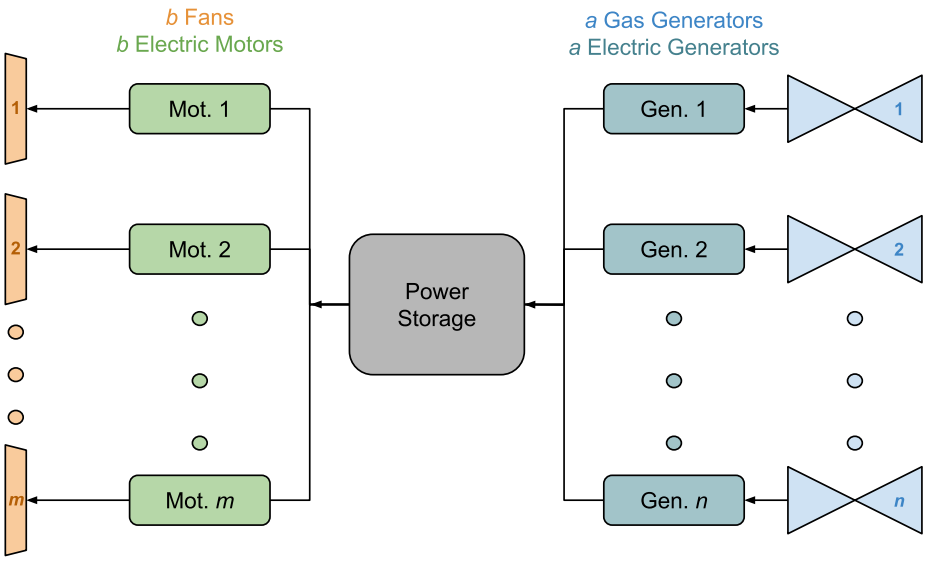

Figure A.1: Turboelectric architecture with a gas generators powering b distributed fans.

defined as

$$\epsilon_{tot}^{elec} = \sum_{i=1}^{a} \left[\eta_{gen}\eta_{pt}E_p\eta_{gg}H_p^{gg}\right]_i \tag{A.2}$$

The first term in Equation (A.1) represents contributions of each gas generator jet while the second term represents the fan contributions. For this model, we assume electrical power is distributed evenly to all motors. However, an equally valid solution would be obtained if a weighted sum of motor input power was used instead.

A.2 Water recovering/recycling turbofan

A diagram of a water-enhanced turbofan engine [41], [42] is shown in Figure A.2. In this system, water is injected into the core stream just before the burner. The resulting flow that exits the gas generator passes through a power turbine as the main fan power source before going through two heat exchangers. The first heats recycled water while the second adds flow power to the bypass stream. The core flow then has the water condensed out and recovered. The recovered water is then charged in a pump, heated in the first heat exchanger, and passed through a steam turbine that powers a) the pump and b) the bypass fan. The water is then reinjected. The MEM expression for this sytem is complex, and is

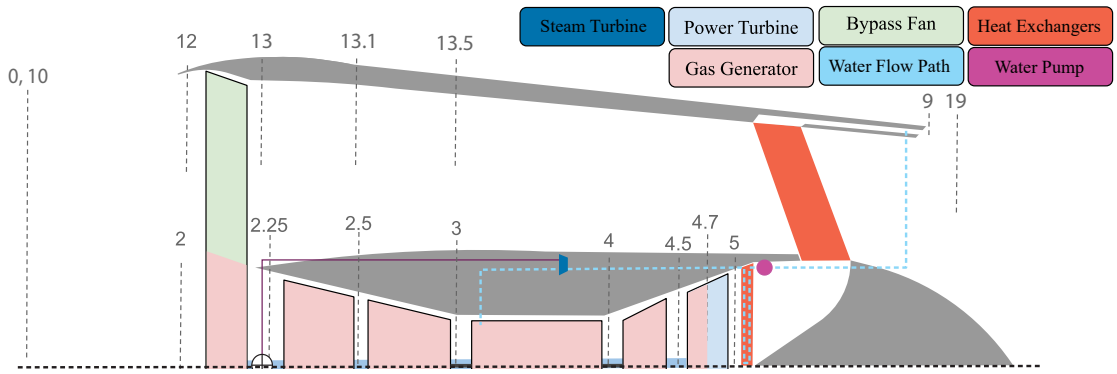

Figure A.2: Axisymmetric view of water recovery/recycling turbofan architecture.

broken into pieces below. As the only source power for the system is fuel, $H_p^{gg} = 1$ and is thus not included in the expression. At the highest level, the MEM expression is

$$\eta_0 = \left[(1 - B_p)(1 - E_p^{he,2})\epsilon_{core} + \epsilon_{water}\right] + \left[\eta_{fan}\eta_{diff}\left[\epsilon_{pt} + \epsilon_{steam}\right] + \eta_{he,2}E_p^{he,2}\epsilon_{core}\right] \quad \text{(A.3)}$$

This is a sum of four primary terms. The first represents the core stream contributions due to the gas generator, parameterized by the ϵ_{core} term. This term takes the form:

$$\epsilon_{core} = (1 - E_p^{he,1})(1 - E_p^{pt})\eta_{gg} \quad \text{(A.4)}$$

The second term, ϵ_{water}, represents the recovery of the water being reinjected into the core stream. Here, the water recovery is assumed to be a perfect process such that none of the circulating water is lost. As such, this term is simply $\epsilon_{water} = \sigma_{water}/P_{tot}$ where σ_{water} is the flow power of the injected water. These two terms are grouped to represent total core stream contributions, while the latter two represent the bypass contributions. The third term represents the fan contribution to the bypass stream, which receives shaft power summed through a mechanical differential from the power turbine and the steam turbine. The contribution from the power turbine takes the established form,

$$\epsilon_{pt} = \eta_{pt}E_p^{pt}\eta_{gg} \quad \text{(A.5)}$$

The ϵ_{steam} term, however, is more complicated. To resolve this term, we assume the recovery stream has a psuedo-gas generator consisting of the pump, heat exchanger, and the portion of the steam turbine used to power the pump. In this way, the system is analogous to a compressor, burner, and turbine conventional gas generator. It then has a gas generator efficiency, defined as:

$$\eta_{steam,gg} = \frac{\Delta\sigma_{steam,gg}}{\Delta\sigma_{he,1}} \tag{A.6}$$

Using this representation and assuming the remainder of the steam turbine functions as a power turbine with extraction fraction E_p^{steam}, ϵ_{steam} becomes:

$$\epsilon_{steam} = \eta_{st} E_p^{steam} \eta_{steam,gg} E_p^{he,1} (1 - E_p^{pt}) \eta_{gg} \tag{A.7}$$

To summarize, the MEM expression for the water injection cycle described is:

$$\eta_0 = \left[(1 - B_p)(1 - E_p^{he,2})\epsilon_{core} + \epsilon_{water} \right] + \left[\eta_{fan}\eta_{diff} \left[\epsilon_{pt} + \epsilon_{steam} \right] + \eta_{he,2} E_p^{he,2} \epsilon_{core} \right] \tag{A.8}$$

$$\epsilon_{core} = (1 - E_p^{he,1})(1 - E_p^{pt})\eta_{gg} \tag{A.9}$$

$$\epsilon_{water} = \frac{\sigma_{water}}{P_{tot}} \tag{A.10}$$

$$\epsilon_{pt} = \eta_{pt} E_p^{pt} \eta_{gg} \tag{A.11}$$

$$\epsilon_{steam} = \eta_{st} E_p^{steam} \eta_{steam,gg} E_p^{he,1} (1 - E_p^{pt}) \eta_{gg} \tag{A.12}$$

Appendix B

Flow Power Versus Exergy

While specific expanded flow power ($\hat{\sigma}$) and specific exergy (x) both measure the useful energy we can extract from a fluid, flow power assumes that a flow can only be expanded to ambient pressure. As such, there is some availability that we cannot extract by bringing the flow to ambient temperature as we would to calculate exergy. Schmitz and Hornung (2013) provide the definition of exergy [15]:

$$x = h_t - h_0 - T_0(s_t - s_0)$$

where state 0 represents the ambient environment. Thus, we write the useful work not captured by flow power as

$$x - \hat{\sigma} = (h_t - h_0 - T_0(s_t - s_0)) - (h_t - h\big|_{p=p_0}) \tag{B.1}$$

$$x - \hat{\sigma} = h\big|_{p=p_0} - h_0 - T_0(s_t - s_0) \tag{B.2}$$

From the Gibbs equation [43], we know that an isobaric process at ambient temperature with $c_p \approx const$ will have entropy and enthalpy related by

$$h(s) = h_0 e^{(s-s_0)/c_p} \tag{B.3}$$

Using this relationship and defining $\Delta s = s_t - s_0$, the difference in exergy and flow power is written non-dimensionally as

$$\frac{x - \hat{\sigma}}{h_0} = e^{\Delta s/c_p} - \left(1 + \frac{\Delta s}{c_p}\right) \tag{B.4}$$

Bernoulli's inequality [44] and the limit definition of the exponential function [45] can be used to show that this quantity is strictly greater than or equal to 0 for $\Delta s/c_p > -1$. For useful cycles, Δs is always greater than or equal to 0, meaning positivity is guaranteed. This means that expanded flow power and exergy are only equal when $\Delta s = 0$, or when the stagnation quantities are achieved through isentropic compression such that h_0 and h_t occur at the same entropy.

There are some components in propulsion systems which can experience a rise in expanded flow power. Using the definition of exergy above, it can be confirmed that the exergy across these components will strictly decrease. Take the flow mixer characterized by the non-dimensionalized $h - s$ diagram in Figure B.1. For this system, the flow power effectiveness, χ, and the exergy efficiency, ζ, are:

$$\chi_{mix} = 1.025\,, \qquad \zeta = 0.99992$$

While the most general case of a mixer does not have a concise analytical representation, if we assume the input streams have a stagnation pressure ratio approaching one and that the output stream has stagnation pressure approaching the input stagnation pressures, we can demonstrate effectiveness vs efficiency for a simplified case. Conservation of mass and energy tell us

$$\dot{m}_{in,1} + \dot{m}_{in,2} = \dot{m}_{out} \tag{B.5}$$

$$\frac{\dot{m}_{in,1} h_{t,1} + \dot{m}_{in,1} h_{t,2}}{\dot{m}_{out}} = h_{t,out} \tag{B.6}$$

If we define $h_{t,1} \gg h_{t,2}$ as in the figure above, the assumption that $p_{t,1} \approx p_{t,2}$ and that $p_{t,out} \to p_{t,1}$ guarantees that $s_{t,1} > s_{t,out} > s_{t,2}$. The exergy can be expressed in terms of

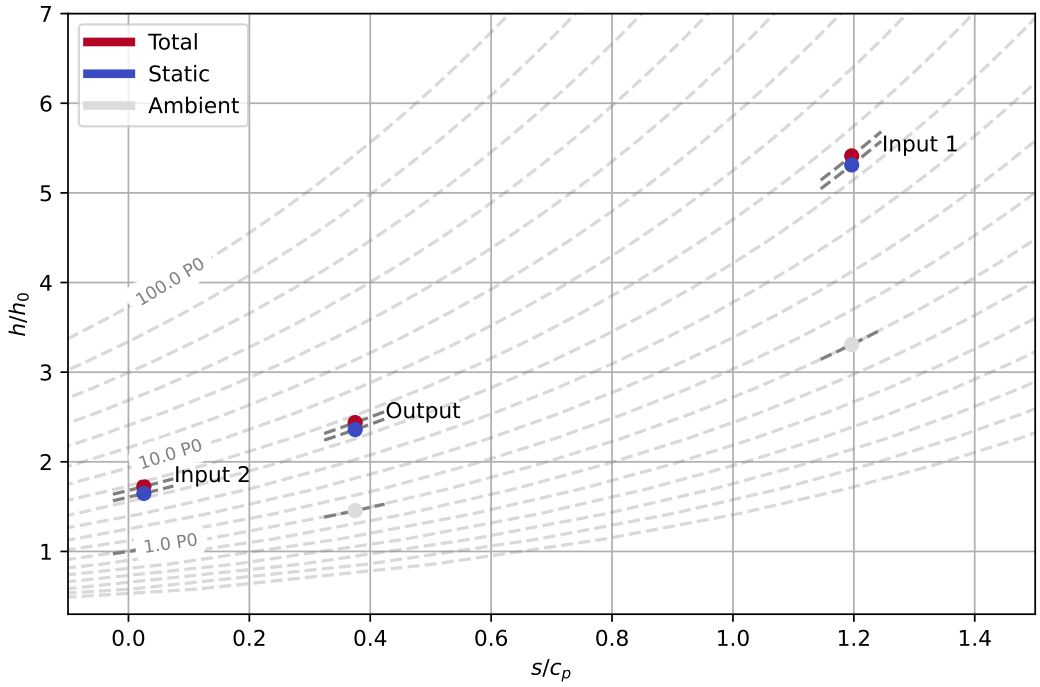

Figure B.1: Non-dimensionalized $h - s$ diagram of a two-stream flow mixer.

entropy difference ($\Delta s = s - s_0$) as:

$$\frac{x}{h_0} = \tau_0 e^{\Delta s/c_p} - 1 - \frac{\Delta s}{c_p} \tag{B.7}$$

where $\tau_0 = h_{t,0}/h_0$. We know that $e^x - (1+x) \geq 0$ on the domain of interest. We also know that the stagnation enthalpy is strictly greater than or equal to the static enthalpy such that

$$\tau_0 e^{\Delta s/c_p} > e^{\Delta s/c_p} > 1 + \frac{\Delta s}{c_p} \tag{B.8}$$

for all physically possible τ_0 values. In addition, we know the normalized exergy is strictly increasing for $\Delta s > 0$ based on positivity of the first derivative:

$$\frac{d}{d(\Delta s/c_p)} \frac{x}{h_0} = \tau_0 e^{\Delta s/c_p} - 1 > 0 \quad \forall \;\; \Delta s > 0 \tag{B.9}$$

As such, if $s_{t,1} > s_{t,out} > s_{t,2}$, then $x_{in,1} > x_{out} > x_{in,2}$, we find that

$$x_{out} < x_{in,1} + x_{in,2} \tag{B.10}$$

$$\eta_{exergy} = \frac{x_{out}}{x_{in,1} + x_{in,2}} < 1 \tag{B.11}$$

From this, we can say that as long as the pressures are arbitrarily close, net exergy will always decrease across a flow mixer. This also applies to leakage bleeds, which are effectively flow mixers.

Appendix C

Estimation of Wave Drag Penalties for SST Engines

Variation in wave drag for the SST engines examined in the main text is done using wave drag estimates for open-nosed bodies of revolution based on work done by Fraenkel [32] as presented in Seddon and Goldsmith [31]. Specifically, only wave drag is accounted for, while spillage and bypass supersonic drag sources are assumed to be negligible due to either on-design inlet operation or the implementation of a variable geometry inlet. We assume a truncated conical profile defined parametrically in Figure C.1. Specific dimensions for the NASA STCA engines were approximated via image measurements from Berton et al [27] and are tabulated in C.1.

The sensitivity of the inlet drag area ($CDA = C_D A_{ref}$) with respect to the baseline STCA inlet was computed across a range of fan diameters and freestream Mach numbers. It is assumed that the ratio A_c/A_m is constant in all cases, with fan diameter specifying $A_m = \pi(d_{fan}/2)^2$. The results in Figure C.2 show a strong positive sensitivity to fan diameter and a weaker negative sensitivity to Mach number, consistent with wave drag increasing at

Table C.1: SST inlet profile parameter values.

Fan radius, r_m [m]	0.578
Capture radius, r_c [m]	0.462
Capture-to-fan area ratio, A_c/A_m	0.671
Inlet length, ℓ [m]	1.0

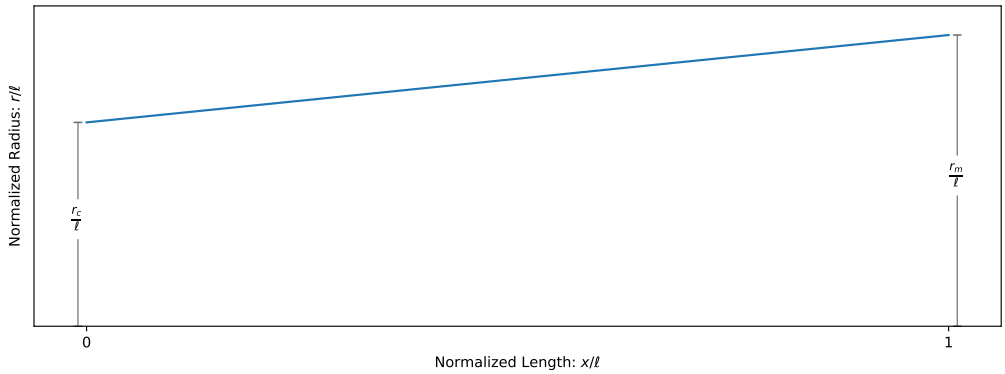

Figure C.1: SST conical inlet profile definition.

Mach numbers close to unity.

This model was incorporated into NPSS by calculating the difference in CDA between the current design and the baseline STCA. The difference in absolute drag per engine was then calculated using freestream conditions and the required thrust was modified by the resulting drag change.

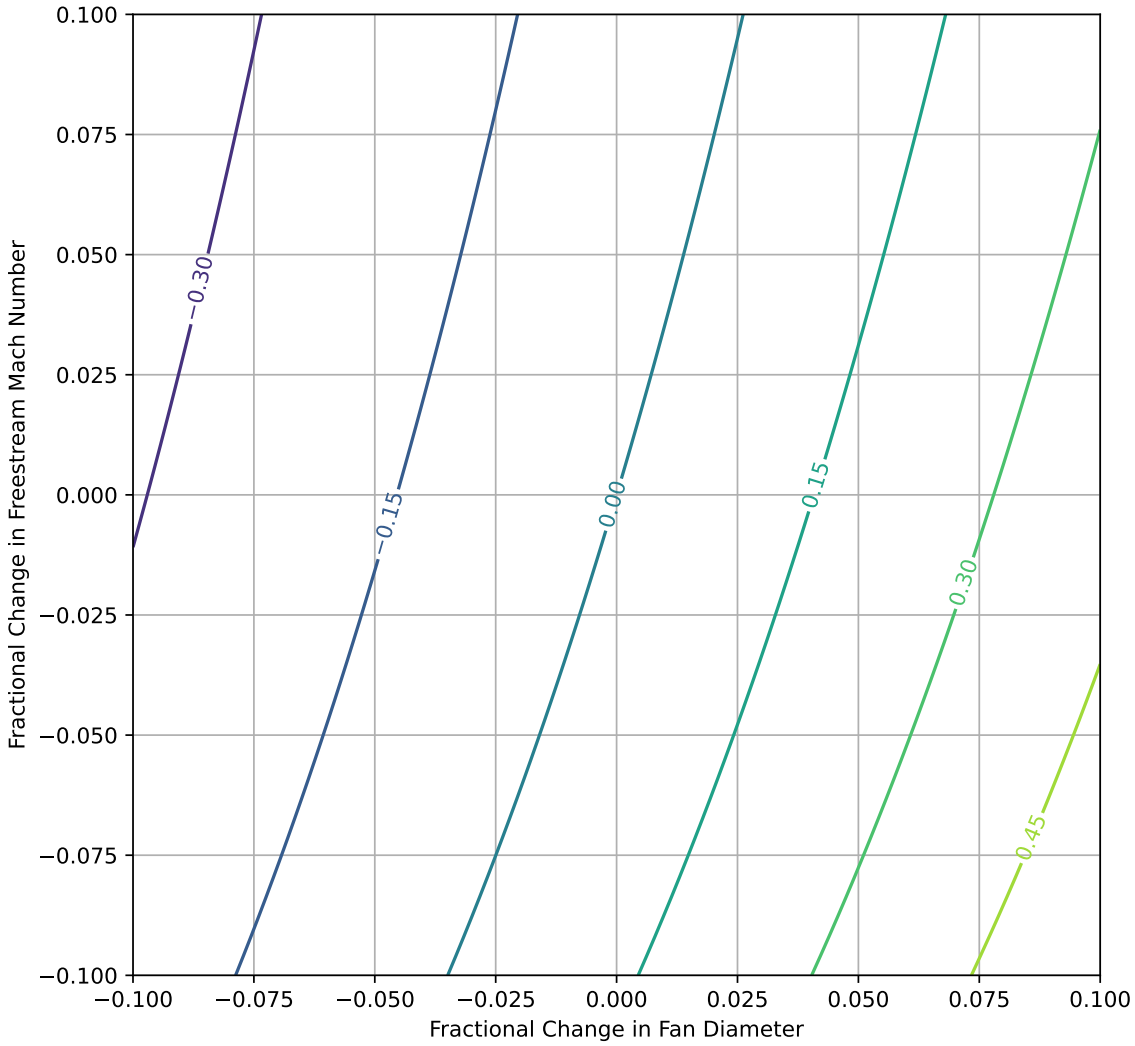

Figure C.2: Contours of fractional change in inlet CDA due to Mach number and fan diameter.

References

[1] *Long term global aspirational goal (LTAG) for international aviation*. URL: https://www.icao.int/environmental-protection/Pages/LTAG.aspx (visited on 03/01/2024).

[2] *States adopt net-zero 2050 global aspirational goal for international flight operations*, Oct. 2022. URL: https://www.icao.int/Newsroom/Pages/States-adopts-netzero-2050-aspirational-goal-for-international-flight-operations.aspx (visited on 04/20/2024).

[3] *Working to Build a Net-Zero Sustainable Aviation System by 2050 | Federal Aviation Administration*, Mar. 2024. URL: https://www.faa.gov/sustainability (visited on 04/20/2024).

[4] *Waypoint 2050*. URL: https://aviationbenefits.org/environmental-efficiency/climate-action/waypoint-2050/ (visited on 03/01/2024).

[5] D. Williams, "2021 United States Aviation Climate Action Plan," 2021. URL: https://www.faa.gov/sites/faa.gov/files/2021-11/Aviation_Climate_Action_Plan.pdf (visited on 05/14/2024).

[6] C. E. Lents, L. W. Hardin, J. Rheaume, and L. Kohlman, "Parallel Hybrid Gas-Electric Geared Turbofan Engine Conceptual Design and Benefits Analysis," in *52nd AIAA/SAE/ASEE Joint Propulsion Conference*, Salt Lake City, UT: American Institute of Aeronautics and Astronautics, Jul. 2016. DOI: 10.2514/6.2016-4610.

[7] A. Seitz, M. Nickl, A. Stroh, and P. C. Vratny, "Conceptual study of a mechanically integrated parallel hybrid electric turbofan," *Proceedings of the Institution of Mechanical Engineers, Part G: Journal of Aerospace Engineering*, vol. 232, no. 14, pp. 2688–2712, Nov. 2018. DOI: 10.1177/0954410018790141.

[8] M. Hoogreef, R. Vos, R. de Vries, and L. L. Veldhuis, "Conceptual Assessment of Hybrid Electric Aircraft with Distributed Propulsion and Boosted Turbofans," in *AIAA Scitech 2019 Forum*, San Diego, California: American Institute of Aeronautics and Astronautics, Jan. 2019. DOI: 10.2514/6.2019-1807.

[9] W. Lammen and J. Vankan, "Energy Optimization of Single Aisle Aircraft with Hybrid Electric Propulsion," in *AIAA Scitech 2020 Forum*, Orlando, FL: American Institute of Aeronautics and Astronautics, Jan. 2020. DOI: 10.2514/6.2020-0505.

[10] M. R. van Holsteijn, A. Gangoli Rao, and F. Yin, "Operating Characteristics of an Electrically Assisted Turbofan Engine," in *GT2020*, V001T01A028, Volume 1: Aircraft Engine; Fans and Blowers, Sep. 2020. DOI: 10.1115/GT2020-15355.

[11] S. Vouros, M. Kavvalos, S. Sahoo, and K. Kyprianidis, "Enabling the potential of hybrid electric propulsion through lean-burn-combustion turbofans," *Journal of the Global Power and Propulsion Society*, vol. 5, pp. 164–176, Sep. 2021. DOI: 10.33737/jgpps/140592.

[12] S. Kang, I. Roumeliotis, J. Zhang, O. Broca, and V. Pachidis, "Assessment of Engine Operability and Overall Performance for Parallel Hybrid Electric Propulsion Systems for a Single-Aisle Aircraft," *Journal of Engineering for Gas Turbines and Power*, vol. 144, no. 4, Jan. 2022. DOI: 10.1115/1.4052880.

[13] J. L. Kerrebrock, "Introduction to Concepts," in *Aircraft Engines and Gas Turbines*, 2nd ed., MIT Press, 1992, pp. 1–28, ISBN: 0-262-27705-0.

[14] J. L. Kerrebrock, "Cycle Analysis with Losses," in *Aircraft Engines and Gas Turbines*, 2nd ed., MIT Press, 1992, pp. 72–103, ISBN: 0-262-27705-0.

[15] O. Schmitz and M. Hornung, "Unified Applicable Propulsion System Performance Metrics," *Journal of Engineering for Gas Turbines and Power*, vol. 135, no. 111201, Sep. 2013. DOI: 10.1115/1.4025066. (visited on 03/12/2024).

[16] J. C. Gladin, D. Trawick, D. N. Mavris, M. J. Armstrong, D. Bevis, and K. Klein, "Fundamentals of Parallel Hybrid Turbofan Mission Analysis with Application to the Electrically Variable Engine," en, in *2018 AIAA/IEEE Electric Aircraft Technologies*

Symposium, Cincinnati, Ohio: American Institute of Aeronautics and Astronautics, Jul. 2018. DOI: 10.2514/6.2018-5024.

[17] A. Seitz, A. Isikveren, and M. Hornung, *Pre-Concept Performance Investigation of Electrically Powered Aero-Propulsion Systems*. Jul. 2013, Journal Abbreviation: 49th AIAA/ASME/SAE/ASEE Joint Propulsion Conference. Publication Title: 49th AIAA/ASME/SAE/ASEE Joint Propulsion Conference. DOI: 10.2514/6.2013-3608.

[18] T. Nam, D. Soban, and D. Mavris, "Power Based Sizing Method for Aircraft Consuming Unconventional Energy," in *43rd AIAA Aerospace Sciences Meeting and Exhibit*, Reno, Nevada: American Institute of Aeronautics and Astronautics, Jan. 2005. DOI: 10.2514/6.2005-818.

[19] M. Hepperle, "Electric Flight - Potential and Limitations," in *Energy Efficient Technologies and Concepts of Operation*, Oct. 2012. URL: https://elib.dlr.de/78726/ (visited on 05/14/2024).

[20] S. M. Jones, "An Introduction to Thermodynamic Performance Analysis of Aircraft Gas Turbine Engine Cycles Using the Numerical Propulsion System Simulation Code," Tech. Rep. NASA/TM-2007-214690, Mar. 2007, NTRS Author Affiliations: NASA Glenn Research Center. NTRS Document ID: 20070018165. NTRS Research Center: Glenn Research Center (GRC). URL: https://ntrs.nasa.gov/citations/20070018165 (visited on 05/14/2024).

[21] L. Lorenz, A. Seitz, and H. Kuhn, "Hybrid Power Trains for Future Mobility," vol. Paper ID 301316, Stuttgart, Germany, Sep. 2013. DOI: 10.13140/2.1.2741.7925.

[22] K. Lee, D. Salgado, P. Prashanth, R. Speth, J. Sabnis, S. Eastham, and S. Barrett, "Influence of Turbofan Engine Design Parameters on Aircraft Environmental Impact," in *AIAA SCITECH 2024 Forum*, Orlando, FL, Jan. 2024. DOI: 10.2514/6.2024-0735.

[23] P. Prashanth, L. Voet, R. Speth, J. Sabnis, C. Tan, and S. Barrett, "The impact of design space constraints on the noise and emissions from derivative engines for civil supersonic aircraft," in *AIAA Scitech 2021 Forum*, Jan. 2021. DOI: 10.2514/6.2021-1272.

[24] T. MacDonald, M. Clarke, E. M. Botero, J. M. Vegh, and J. J. Alonso, "SUAVE: An Open-Source Environment Enabling Multi-Fidelity Vehicle Optimization," in *18th AIAA/ISSMO Multidisciplinary Analysis and Optimization Conference*, Denver, Colorado: American Institute of Aeronautics and Astronautics, Jun. 2017. DOI: 10.2514/6.2017-4437.

[25] M. Daly, *Jane's Aero-Engines (2019-2020)*. Coulsdon, Surrey : Jane's Group UK Limited, 2019, vol. 2018-2019, ISSN: 2516-5313.

[26] J. J. Berton, D. L. Huff, K. Geiselhart, and J. Seidel, "Supersonic Technology Concept Aeroplanes for Environmental Studies," in *AIAA Scitech 2020 Forum*, Orlando, FL: American Institute of Aeronautics and Astronautics, Jan. 2020. DOI: 10.2514/6.2020-0263.

[27] J. Berton, D. Huff, J. Seidel, and K. Geiselhart, "NASA 55 tonne Supersonic Transport Concept Aeroplane (STCA) Release Package," Feb. 2020. (visited on 05/14/2024).

[28] P. Virtanen, R. Gommers, T. E. Oliphant, *et al.*, "SciPy 1.0: Fundamental Algorithms for Scientific Computing in Python," *Nature Methods*, vol. 17, pp. 261–272, 2020. DOI: 10.1038/s41592-019-0686-2.

[29] *Python 3.8.18 Documentation*, Feb. 2024. URL: https://docs.python.org/3.8/ (visited on 04/19/2024).

[30] *StartupBoeing*, en-US, 2024. URL: https://www.boeing.com/content/theboeingcompany/us/en/company/about-bca/startupboeing (visited on 04/19/2024).

[31] J. Seddon and E. L. Goldsmith, *Intake aerodynamics* (AIAA education series). New York, N.Y: American Institute of Aeronautics and Astronautics, 1985, ISBN: 0-930403-03-7.

[32] L. E. Fraenkel, "The Theoretical Wave-Drag of Some Bodies of Revolution," British R.A.E, Rep. No. Aero 2420, May 1951.

[33] G. C. Oates, "Performance estimation for turbofans with and without mixers," *Journal of Propulsion and Power*, vol. 1, no. 3, pp. 252–256, May 1985. DOI: 10.2514/3.22788.

[34] R. J. Pera, E. Onat, G. W. Klees, and E. Tjonneland, "A method to estimate weight and dimensions of aircraft gas turbine engines. Volume 1: Method of analysis," Tech. Rep. D6-44258-VOL-1, May 1977, NTRS Author Affiliations: Boeing Co. NTRS Document ID: 19770018227. NTRS Research Center: Legacy CDMS (CDMS). URL: https://ntrs.nasa.gov/citations/19770018227 (visited on 05/14/2024).

[35] *Density of steel*. URL: https://www.pipingmaterial.ae/blog/density-of-steel/ (visited on 04/19/2024).

[36] A. J. B. Jackson, "Optimisation of Aero and Industrial Gas Turbine Design For The Environment," Ph.D. dissertation, Cranfield University, Feb. 2009. URL: https://dspace.lib.cranfield.ac.uk/bitstream/handle/1826/4316/A_J_B_Jackson_Thesis_2009.pdf?sequence=1&isAllowed=y (visited on 04/19/2024).

[37] A. Dowdle, D. K. Hall, and J. Lang, "Electric Propulsion Architecture Assessment via Signomial Programming," in *2018 AIAA/IEEE Electric Aircraft Technologies Symposium*, Cincinnati, Ohio: American Institute of Aeronautics and Astronautics, Jul. 2018. DOI: 10.2514/6.2018-5026.

[38] Z. Šimić, D. Topić, G. Knežević, and D. Pelin, "Battery energy storage technologies overview," *International journal of electrical and computer engineering systems*, vol. 12, no. 1, pp. 53–65, Apr. 2021. DOI: 10.32985/ijeces.12.1.6.

[39] J. H. Horlock and L. Torbidoni, "Calculations of Cooled Turbine Efficiency," *Journal of Engineering for Gas Turbines and Power*, vol. 130, no. 011703, Jan. 2008. DOI: 10.1115/1.2771250.

[40] J. Hartsel, "Prediction of effects of mass-transfer cooling on the blade-row efficiency of turbine airfoils," in *10th Aerospace Sciences Meeting*, ser. Aerospace Sciences Meetings, American Institute of Aeronautics and Astronautics, Jan. 1972. DOI: 10.2514/6.1972-11.

[41] S. Kaiser, O. Schmitz, P. Ziegler, and H. Klingels, "The Water-Enhanced Turbofan as Enabler for Climate-Neutral Aviation," *Applied Sciences*, vol. 12, no. 23, 2022. DOI: 10.3390/app122312431.

[42] P. Ziegler, S. Kaiser, and V. Gümmer, "Parametric Cycle Studies of the Water-Enhanced Turbofan Concept," in *GT2023*, V005T06A001, Volume 5: Cycle Innovations, Jun. 2023. DOI: 10.1115/GT2023-100529.

[43] E. M. Greitzer, C. S. Tan, and M. B. Graf, *Internal Flow: Concepts and Applications* (Cambridge Engine Technology Series; 3). Cambridge, UK; New York: Cambridge University Press, 2004, ISBN: 0-521-34393-3.

[44] D. S. Mitrinović, J. E. Pečarić, and A. M. Fink, "Bernoulli's Inequality," in *Classical and New Inequalities in Analysis*, D. S. Mitrinović, J. E. Pečarić, and A. M. Fink, Eds., Dordrecht: Springer Netherlands, 1993, pp. 65–81, ISBN: 978-94-017-1043-5. DOI: 10.1007/978-94-017-1043-5_3.

[45] M. Abramowitz and I. Stegun, "Handbook of Mathematical Functions with Formulas, Graphs, and Mathematical Tables," in Section: 4.2 Exponential Function, U.S. Department of Commerce, NIST, 1972, pp. 69–70. URL: https://app.knovel.com/hotlink/pdf/id:kt00A81I5B/handbook-mathematical/exponential-function.